Adv Comput Math (2021) 47:85
https://doi.org/10.1007/s10444-021-09911-5

The hot spots conjecture can be false: some numerical examples

Andreas Kleefeld[1]

Received: 27 January 2021 / Accepted: 8 November 2021 / Published online: 04 December 2021
© The Author(s) 2021

Abstract
The hot spots conjecture is only known to be true for special geometries. This paper shows numerically that the hot spots conjecture can fail to be true for easy to construct bounded domains with one hole. The underlying eigenvalue problem for the Laplace equation with Neumann boundary condition is solved with boundary integral equations yielding a non-linear eigenvalue problem. Its discretization via the boundary element collocation method in combination with the algorithm by Beyn yields highly accurate results both for the first non-zero eigenvalue and its corresponding eigenfunction which is due to superconvergence. Additionally, it can be shown numerically that the ratio between the maximal/minimal value inside the domain and its maximal/minimal value on the boundary can be larger than $1 + 10^{-3}$. Finally, numerical examples for easy to construct domains with up to five holes are provided which fail the hot spots conjecture as well.

Keywords Interior Neumann eigenvalues · Helmholtz equation · Potential theory · Boundary integral equations · Numerics

Mathematics Subject Classification (2010) 35J25 · 35P20 · 65F15 · 65M38

1 Introduction

The hot spots conjecture has been given in 1974 by Jeffrey Rauch [31] and explicitly stated a decade later in Kawohl [17]. Refer also to the paper by Bañuelos &

Communicated by: Michael O'Neil

This article belongs to the Topical Collection: *Advances in Computational Integral Equations*
Guest Editors: Stephanie Chaillat, Adrianna Gillman, Per-Gunnar Martinsson, Michael O'Neil, Mary-Catherine Kropinski, Timo Betcke, Alex Barnett

✉ Andreas Kleefeld
a.kleefeld@fz-juelich.de

[1] Forschungszentrum Jülich GmbH, Jülich Supercomputing Centre, 52425 Jülich, Germany

Burdzy [6] from 1999. Since then a lot of researchers have worked on this challenging problem (see Judge & Mondal [16] for a recent overview from 2020).

Before stating it in mathematical terms, we explain it in a simple fashion. Imagine that we have a flat piece of metal D where D is a bounded subset of the two-dimensional space (Euclidean domain) which can have holes with a sufficiently smooth boundary. Next, an (almost) arbitrary initial temperature distribution is provided on D (refer to [6, p. 2]). Assume that the domain is insulated, then the hottest and coldest spot of D will appear on the boundary when waiting for a long time.

Now, we go into the mathematical detail: That means we have to solve the heat equation $\partial_t u = \Delta u$ for large t with homogeneous Neumann boundary condition $\partial_\nu u = 0$ and 'almost' arbitrary initial condition in an open connected bounded D with Lipschitz boundary (see [6, p. 2] and [33] for the definition of a Lipschitz domain). Refer to Fig. 1 for an example.

Precisely, we have to find the smallest non-trivial eigenvalue of the Laplacian with homogeneous Neumann boundary condition and the corresponding eigenfunction. Note that the smallest eigenvalue of the Laplacian with homogeneous Neumann boundary condition is zero with corresponding eigenfunction $u_0 = \text{const}$. Mathematically, we have to find a solution $u \neq 0$ and the smallest $k \in \mathbb{R}_{>0}$ such that the Helmholtz equation $\Delta u + k^2 u = 0$ in D with $\partial_\nu u = 0$ on the boundary Γ. All solutions k are called non-trivial interior Neumann eigenvalues and $\lambda_i = k_i^2$ will be the ith non-trivial Neumann eigenvalue of the Laplacian. Its corresponding eigenfunctions are denoted by u_i. Further, it is known that the eigenvalues satisfy $0 = \lambda_0 < \lambda_1 \leq \lambda_2 \leq \lambda_3 \leq \ldots$ when D is a bounded planar domain with Lipschitz boundary (see for example [14, p. 449] and the references therein, specifically [32]). If $\lambda_1 < \lambda_2$ and $\langle u(0,\cdot), u_1\rangle \neq 0$, then $u(t,x) = C + \mathrm{e}^{-\lambda_1 t}\langle u(0,\cdot), u_1\rangle u_1(x) +$ lower terms. Note that the first non-trivial eigenvalue can have multiplicity more than one which means that there can be more than one eigenfunction.

Now, the conjecture can be stated as (refer also to [6, p. 2]): Let $D \subset \mathbb{R}^2$ be an open connected bounded domain with Lipschitz boundary Γ. Then:

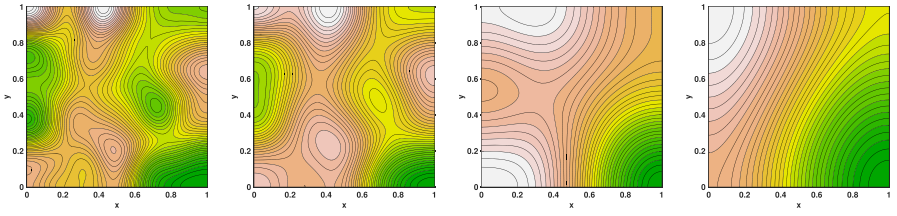

(a) Solution at time $t_1 = 1/200$ (b) Solution at time $t_2 = 1/10$ (c) Solution at time $t_3 = 1/2$ (d) Solution at time $t_4 = 2$

Fig. 1 The numerical solution of the heat equation $\partial_t u = \frac{1}{10}\Delta u$ and initial condition with standard normal random numbers and homogeneous Neumann boundary condition for time $t_1 = 1/200$, $t_2 = 1/10$, $t_3 = 1/2$, and $t_4 = 2$ using $h = 1/100$ and $k = 1/100$ (see also [2, p. 11] for more details on the implementation of the exponential time differencing method). The maximal and minimal value for T_4 appear on the boundary. Note that the solution T_4 is approximately representing the first non-zero Neumann eigenfunction (see [20, Figure 9 (a)])

C1: For each eigenfunction $u_1(x)$ corresponding to λ_1 that is not identically zero, we have

$$\inf_{x\in\Gamma} u_1(x) < u_1(y) < \sup_{x\in\Gamma} u_1(x) \quad \forall y \in D\,.$$

C2: For each eigenfunction $u_1(x)$ corresponding to λ_1 that is not identically zero, we have

$$\inf_{x\in\Gamma} u_1(x) \leq u_1(y) \leq \sup_{x\in\Gamma} u_1(x) \quad \forall y \in D\,.$$

C3: There exists an eigenfunction $u_1(x)$ corresponding to λ_1 that is not identically zero, such that

$$\inf_{x\in\Gamma} u_1(x) \leq u_1(y) \leq \sup_{x\in\Gamma} u_1(x) \quad \forall y \in D\,.$$

Here, C1 is the original conjecture of Rauch. The hypothesis has been shown to be true for some special geometries such as parallelepipeds, balls, rectangles, cylinders [17], obtuse triangles [6], some convex and non-convex domains with symmetry [6], wedges [3], lip domains [4], convex domains with two axes of symmetry [15], convex $C^{1,\alpha}$ domains ($0 < \alpha < 1$) with one axis of symmetry [30], a certain class of planar convex domains [28], subequilateral isosceles triangles [29], a certain class of acute triangles [36], Euclidean triangles [16], and strips on two-dimensional Riemannian manifolds [24].

It is assumed that the hot spots conjecture is true for arbitrary convex domains, but a proof is still open. The hot spots conjecture is assumed to be true also for simply connected bounded non-convex domains, but no successful attempts (neither theoretically nor numerically) have been made to prove this conjecture or to find a counter-example.

It has been shown that for some domains with one hole that the hot spots conjecture is true (for example an annulus [17]), but that there are also domains with one or more holes where the hot spots conjecture is false (see Burdzy [9], Burdzy & Werner [10], and Bass & Burdzy [7], respectively). For domains on manifolds, we refer the reader to [13].

The proofs in [7, 9, 10] are very technical and are based on stochastic arguments. Further, the constructed domain is too complicated in order to provide numerical results with the boundary element collocation method due to the following three facts: (i) the boundary of the domain consists of a polygonal part, (ii) the boundary of the domain consists of polygonal Jordan arcs satisfying certain angular conditions, and (iii) parts of the domain are very thin.

The only non-published numerical results given so far are for triangles in the Poly-Math project 7 ‘Hot spots conjecture’ from 2012 to 2013 using the finite element method.

Further work in the direction of better understanding the conjecture is given for example by Steinerberger [39]. Related results on graphs are given by Lederman & Steinerberger [26].

2 Contribution

It is the goal of this paper to construct 'simple' domains with one hole inspired by Burdzy's work [9] and show numerically with high precision (due to superconvergence) that those domains do not satisfy the hot spots conjecture. For simplicity, we restrict our attention to domains with sufficiently smooth boundaries (at least of class C^1), but the results could also be extended to domains with Lipschitz boundaries (see [20] for more details). The method based on boundary integral equations is very efficient and its convergence is faster than expected. Additionally, we show the influence on the location of the hot spots by changing the boundary of the domain in order to understand this connection. Precisely, we show that symmetry is not needed to show the failure of the hot spots conjecture, but if the deviation is too large, then the hot spots conjecture holds. Further, certain assumptions given in Burdzy's domain such that $\varepsilon_0 < \varepsilon$ might be removable. It is believed that this work might help researchers to provide assumptions when the hot spots conjecture will be true or false for arbitrary bounded simply connected domains which are not necessarily convex. We show that it is possible to construct domains with one hole such that the ratio between the maximum/minimum in the interior and its maximum/minimum on the boundary is larger than $1 + 10^{-3}$. Finally, numerical results are given that show that there exist domains with up to five holes which do not satisfy the hot spots conjecture as well. The Matlab programs including the produced data are available at github https://github.com/kleefeld80/hotspots and can be used by any researcher trying their own geometries and to reproduce the numerical results within this article.

3 Outline of the paper

In Section 4, we explain the algorithm in order to compute the first non-zero Neumann Laplace eigenvalue and its corresponding eigenfunction for an arbitrary domain with or without a hole using boundary integral equations resulting in a non-linear eigenvalue problem. Further, it is shown in detail how to discretize the boundary integral equations via the boundary element collocation method and how to numerically solve the non-linear eigenvalue problem. Extensive numerical results are provided in Section 5 showing the superconvergence and highly accurate results for domains with one or no hole. Domains are provided that show the failure of the hot spots conjecture and further interesting results. The extension to domains with up to five holes is straightforward and given at the end of this section as well. A short summary and outlook is given in Section 6.

4 The algorithm

In this section, we explain the algorithm to compute numerically non-trivial interior Neumann eigenvalues and its corresponding eigenfunction to high accuracy for

bounded domains with one hole (the extension to more than one hole is straightforward) very efficiently. The ingredients are boundary integral equations and its approximation via boundary element collocation method; that is, a two-dimensional problem is reduced to a one-dimensional problem. The resulting non-linear eigenvalue problem is solved using complex-valued contour integrals integrating over the resolvent reducing the non-linear eigenvalue problem to a linear eigenvalue problem which is possible due to Keldysh's theorem (see Beyn [8]).

4.1 Notations

We consider a bounded domain $D \subset \mathbb{R}^2$ with one hole. The outer boundary Γ_1 is assumed to be sufficiently smooth (at least of class C^1) that is oriented counterclockwise and a sufficiently smooth (at least of class C^1) inner boundary Γ_2 that is oriented clockwise. The normal ν_1 on the boundary Γ_1 is pointing into thev unbounded exterior E. The normal ν_2 on the boundary Γ_2 is pointing into the bounded exterior I. We refer the reader to Fig. 2. The boundary of D is given by $\Gamma = \Gamma_1 \cup \Gamma_2$ ($\Gamma_1 \cap \Gamma_2 \neq \emptyset$).

Note that we also consider bounded domains without a hole. In this case, we have $\Gamma_2 = \emptyset$ and hence $\Gamma = \Gamma_1$ and $I = \emptyset$.

4.2 Boundary integral equation

The solution to the Helmholtz equation $\Delta u + k^2 u = 0$ (reduced wave equation) in the domain D for a given wave number k with $\mathrm{Im}(k) \geq 0$ is given by (see [12, Theorem 2.1])

$$u(x) = \int_\Gamma \partial_{\nu(y)} u(y) \cdot \Phi_k(x, y) - u(y) \cdot \partial_{\nu(y)} \Phi_k(x, y) \, \mathrm{d}s(y), \quad x \in D$$

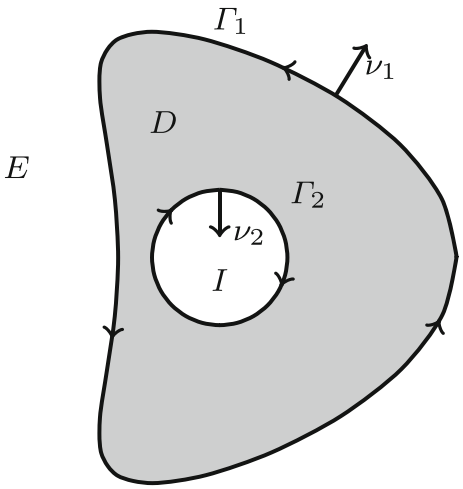

Fig. 2 Used notations for a bounded domain with one hole

which can be written in our notation as

$$u(x) = \int_{\Gamma_1} \partial_{\nu_1(y)} u(y) \cdot \Phi_k(x, y) - u(y) \cdot \partial_{\nu_1(y)} \Phi_k(x, y) \, \mathrm{d}s(y) + \int_{\Gamma_2} \partial_{\nu_2(y)} u(y) \cdot \Phi_k(x, y) - u(y) \cdot \partial_{\nu_2(y)} \Phi_k(x, y) \, \mathrm{d}s(y), \quad x \in D \tag{1}$$

where $\Phi_k(x, y) = \mathrm{i} H_0^{(1)}(k\|x - y\|)/4$, $x \neq y$ denotes the fundamental solution of the Helmholtz equation in two dimensions (see [12, p. 66]). Here, $H_0^{(1)}$ denotes the first-kind Hankel function of order zero. We denote $u(y)$ for $y \in \Gamma_1$ as $u_1(y)$ and similarly $u(y)$ for $y \in \Gamma_2$ as $u_2(y)$. Hence, we can write (1) as

$$u(x) = -\int_{\Gamma_1} u_1(y) \cdot \partial_{\nu_1(y)} \Phi_k(x, y) \, \mathrm{d}s(y) - \int_{\Gamma_2} u_2(y) \cdot \partial_{\nu_2(y)} \Phi_k(x, y) \, \mathrm{d}s(y), \quad x \in D \tag{2}$$

where we also used the homogeneous Neumann boundary conditions $\partial_{\nu_1} u = 0$ and $\partial_{\nu_2} u = 0$. We rewrite (2) as

$$u(x) = -\mathrm{DL}_k^{\Gamma_1} u_1(x) - \mathrm{DL}_k^{\Gamma_2} u_2(x), \quad x \in D \tag{3}$$

where we used the notation

$$\mathrm{DL}_k^{\Gamma_i} \psi_i(x) = \int_{\Gamma_i} \psi_i(y) \cdot \partial_{\nu_i(y)} \Phi_k(x, y) \, \mathrm{d}s(y), \quad x \in D, \quad i = 1, 2$$

for the *acoustic double layer potential* with density ψ_i (see [12, p. 39]). Assume for a moment that k is given. The functions u_1 and u_2 are still unknown. Once we know them, we can compute the solution u inside the domain of D at any point we want using (3).

Now, we explain how to obtain those functions u_1 and u_2 on the boundary. Letting $x \in D$ approach the boundary Γ_1 and using the jump relation of the acoustic double layer operator (see [12, p. 39]), yields the boundary integral equation

$$u_1(x) = -\left(\mathrm{D}_k^{\Gamma_1 \to \Gamma_1} u_1(x) - \frac{1}{2} u_1(x) \right) - \mathrm{D}_k^{\Gamma_2 \to \Gamma_1} u_2(x), \quad x \in \Gamma_1 \tag{4}$$

where we used the notation

$$\mathrm{D}_k^{\Gamma_i \to \Gamma_j} \psi_i(x) = \int_{\Gamma_i} \psi_i(y) \cdot \partial_{\nu_i(y)} \Phi_k(x, y) \, \mathrm{d}s(y), \quad x \in \Gamma_j, \quad i, j = 1, 2$$

for the *double layer operator* (see [12, p. 41]).

Similarly, we obtain for $x \in D$ approaching the boundary Γ_2 and using the jump relation for the double layer operator

$$u_2(x) = -\mathrm{D}_k^{\Gamma_1 \to \Gamma_2} u_1(x) - \left(\mathrm{D}_k^{\Gamma_2 \to \Gamma_2} u_2(x) - \frac{1}{2} u_2(x) \right), \quad x \in \Gamma_2. \tag{5}$$

We can rewrite (4) and (5) as a 2×2 system of boundary integral equations in the form

$$\underbrace{\left(\frac{1}{2}\overbrace{\begin{pmatrix} \mathrm{I} & 0 \\ 0 & \mathrm{I} \end{pmatrix}}^{\mathrm{I_B}} + \overbrace{\begin{pmatrix} \mathrm{D}_k^{\Gamma_1\to\Gamma_1} & \mathrm{D}_k^{\Gamma_2\to\Gamma_1} \\ \mathrm{D}_k^{\Gamma_1\to\Gamma_2} & \mathrm{D}_k^{\Gamma_2\to\Gamma_2} \end{pmatrix}}^{\mathrm{K}(k)}\right)}_{\mathrm{M}(k)} \underbrace{\begin{pmatrix} u_1 \\ u_2 \end{pmatrix}}_{u} = \begin{pmatrix} 0 \\ 0 \end{pmatrix} \quad \text{on } \Gamma \tag{6}$$

where I and $\mathrm{I_B}$ denotes the identity and the 2×2 block identity operator, respectively. Hence, we have to numerically solve the non-linear eigenvalue problem (6) written as $\mathrm{M}(k)u = 0$ to find the smallest non-trivial (real) eigenvalue k and the corresponding eigenfunction u. Then, we can numerically evaluate (3) to compute the eigenfunction at any point in the interior we want. As in [19, p. 188], we can argue that the compact operator $\mathrm{K}(k)$ maps from $\mathcal{H}^{-1/2}(\Gamma_1) \times \mathcal{H}^{-1/2}(\Gamma_2)$ to $\mathcal{H}^{1/2}(\Gamma_1) \times \mathcal{H}^{1/2}(\Gamma_2)$. Here, $\mathcal{H}^s(\Gamma)$ denotes a Sobolev space of order $s \in \mathbb{R}$ on the domain Γ which are defined via Bessel potentials (see [27, pp. 75–76] for more details). The operator $\mathrm{M}(k) = \frac{1}{2}\mathrm{I_B} + \mathrm{K}(k)$ is Fredholm of index zero for $k \in \mathbb{C}\backslash\mathbb{R}_{\leq 0}$ and therefore the theory of eigenvalue problems for holomorphic Fredholm operator-valued functions applies to $\mathrm{M}(k)$.

4.3 Discretization

In this section, we explain how to discretize (6) using quadratic interpolation of the boundary, but using piecewise quadratic interpolation (similar as in [21] for the 3D case) instead of quadratic interpolation for the unknown u on each of the n_f boundary elements which ultimately leads to the non-linear eigenvalue

$$\mathbf{M}(k)u = 0 \tag{7}$$

where the matrix is of size $3 \cdot 2 \cdot n_f \times 3 \cdot 2 \cdot n_f$. The size of the matrix is slightly larger than the one given in Kleefeld [19], but it has the advantage that no singular integral has to be evaluated numerically, since we can use a similar singularity subtraction technique as explained in Kleefeld and Lin [22, pp. A1720–A1721] and the convergence rate is slightly higher. The details are about to follow for a domain without a hole for simplicity. In this case, we have to solve a boundary integral equation of the second kind of the form

$$\frac{1}{2}u_1(x) + \int_{\Gamma_1} u_1(y)\partial_{\nu_1(y)}\Phi_k(x,y)\,\mathrm{d}s(y) = 0\,, \quad x \in \Gamma_1\,. \tag{8}$$

First, we subdivide the boundary Γ_1 into n_f pieces denoted by Δ_j with $j = 1, \ldots, n_f$. A subdivision into four pieces is shown in Fig. 3 for the unit circle.

Then equation (8) can be equivalently written as

$$\frac{1}{2}u_1(x) + \sum_{j=1}^{n_f}\int_{\Delta_j} u_1(y)\partial_{\nu_1(y)}\Phi_k(x,y)\,\mathrm{d}s(y) = 0\,, \quad x \in \Gamma_1\,.$$

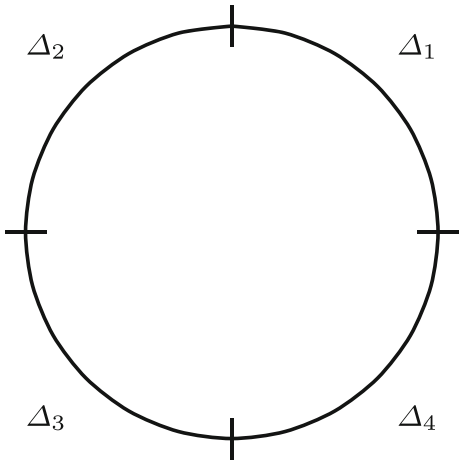

Fig. 3 Subdivision of the given boundary Γ_1 into four pieces Δ_1, Δ_2, Δ_3, and Δ_4

For each j there exists a bijective map m_j which maps from the standard interval $\sigma = [0, 1]$ to Δ_j. Then, we can apply a simple change of variables to each integral over Δ_j giving

$$\frac{1}{2}u_1(x) + \sum_{j=1}^{n_f} \int_\sigma u_1(m_j(s))\partial_{v_1(m_j(s))}\Phi_k(x, m_j(s))J_j(s)\,\mathrm{d}s(s) = 0\,, \quad x \in \Gamma_1$$

with the Jacobian given by $J_j(s) = \|\partial_s m_j(s)\|$. In most cases, we can explicitly write down this map. However, we approximate each $m_j(s)$ by a quadratic interpolation polynomial $m_j(s) \approx \widetilde{m}_j(s) = \sum_{i=1}^{3} v_{((i-1)+2(j-1)) \bmod (2n_f)+1} L_i(s)$ where the Lagrange basis functions are

$$L_1(s) = u\cdot(1-2s)\,, \quad L_2(s) = 4s\cdot u\,, \quad \text{and} \quad L_3(s) = s\cdot(2s-1)$$

with $u = 1 - s$. Here, $\gamma \bmod \delta = \gamma - \lfloor \frac{\gamma}{\delta} \rfloor \cdot \delta$ with $\lfloor\cdot\rfloor$ the floor function. The nodes v_ℓ ($\ell = 1, \ldots, 2n_f$) are the given vertices and midpoints of the n_f faces. We refer the reader to Fig. 4 for an example with four faces and eight nodes (four vertices and midpoints, respectively).

An example how the approximation of Δ_1 via a quadratic interpolation polynomial using two vertices and the midpoint looks like is shown in Fig. 5. Next, we define the 'collocation nodes' $\widetilde{v}_{j,k}$ by $\widetilde{v}_{j,k} = \widetilde{m}_j(q_k)$ for $j = 1, \ldots, n_f$ and for $k = 1, 2, 3$ where $\widetilde{q}_1 = \alpha$, $\widetilde{q}_2 = 1/2$, and $\widetilde{q}_3 = 1 - \alpha$ with $0 < \alpha < 1/2$ a given and fixed constant. This ensures that the collocation nodes are always lying within a piece of the boundary and at those points the interior solid angle is $1/2$. For a specific choice of α the overall convergence rate can be improved. The first three collocation nodes on the approximated boundary for the unit circle using $\alpha = (1 - \sqrt{3/5})/2$ are shown in Fig. 6.

The unknown function $u_1(\widetilde{m}_j(s))$ is approximated on each of the j pieces by a quadratic interpolation polynomial that is of the form $\sum_{k=1}^{3} u_1(\widetilde{m}_j(q_k))\widetilde{L}_k(s)$ which

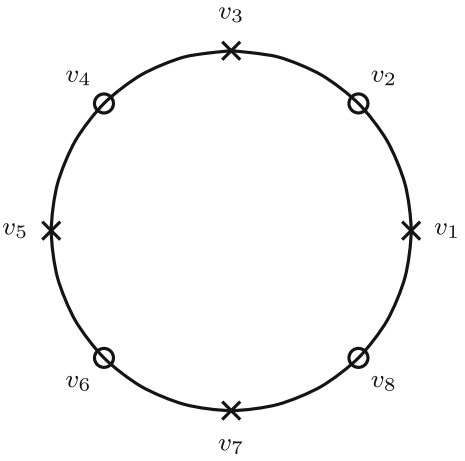

Fig. 4 The eight nodes $v_1, \ldots, v_8$, the four vertices v_1, v_3, v_5, and v_7 (marked with $\times$), and the four midpoints v_2, v_4, v_6, and v_8 (marked with $\circ$) for the four faces Δ_1, Δ_2, Δ_3, and Δ_4

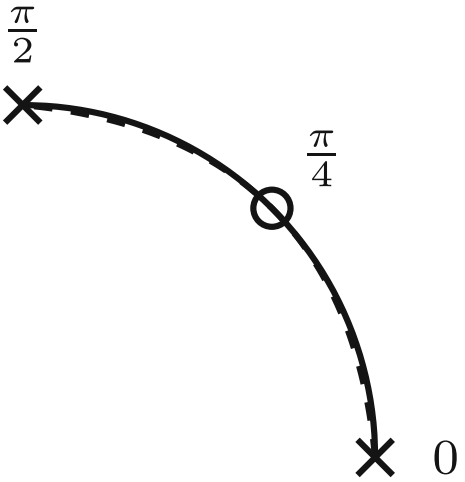

Fig. 5 The approximation of the first part of the boundary Δ_1 (solid line) via a quadratic interpolation polynomial using two vertices and the midpoint (dashed line)

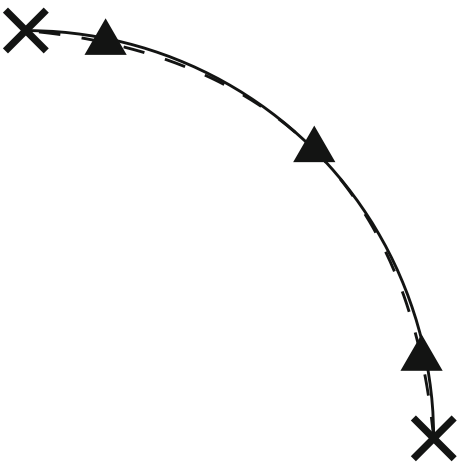

Fig. 6 The first three collocation nodes (solid triangles) on the first part of the approximated boundary (dashed line) for the unit circle using $\alpha = (1 - \sqrt{3/5})/2$. The exact boundary is shown with a solid line including the two vertices marked by a cross

can be written as $\sum_{k=1}^{3} u_1(\widetilde{v}_{j,k})\widetilde{L}_k(s)$ where the Lagrange basis functions are given by

$$\widetilde{L}_1(s) = \frac{u-\alpha}{1-2\alpha}\frac{1-2s}{1-2\alpha}\,,\ \widetilde{L}_2(s) = 4\frac{s-\alpha}{1-2\alpha}\frac{u-\alpha}{1-2\alpha}\,,\ \widetilde{L}_3(s) = \frac{s-\alpha}{1-2\alpha}\frac{2s-1}{1-2\alpha}$$

with $u = 1-s$. We obtain

$$\frac{1}{2}u_1(x) + \sum_{j=1}^{n_f}\sum_{k=1}^{3}\int_{\sigma} \partial_{v_1(\widetilde{m}_j(s))}\Phi_k(x,\widetilde{m}_j(s))\|\partial_s\widetilde{m}_j(s)\|\widetilde{L}_k(s)\,\mathrm{d}s(s)u_1(\widetilde{v}_{j,k}) = r(x)$$

with $r(x)$ the residue which is due to the different approximations. We set $r(\widetilde{v}_{i,\ell}) = 0$ and obtain the linear system of size $3n_f \times 3n_f$

$$\frac{1}{2}u_1(\widetilde{v}_{i,\ell}) + \sum_{j=1}^{n_f}\sum_{k=1}^{3} a_{i,\ell,j,k}u_1(\widetilde{v}_{j,k}) = 0$$

with the resulting integrals

$$a_{i,\ell,j,k} = \int_{\sigma} \partial_{v_1(\widetilde{m}_j(s))}\Phi_k(\widetilde{v}_{i,\ell},\widetilde{m}_j(s))\|\partial_s\widetilde{m}_j(s)\|\widetilde{L}_k(s)\,\mathrm{d}s(s) \tag{9}$$

which will be approximated by the adaptive Gauß-Kronrod quadrature (see [35]). This can be written abstractly as $\mathbf{M}(k)u = 0$. Note that the integrand of the integral of the right-hand side (9) can easily be written down as

$$\frac{\mathrm{i}kH_1^{(1)}(kr)}{4r}\,(a\cdot n_1 + b\cdot n_2)\,\widetilde{L}_k(s)$$

with $H_1^{(1)}$ the first-kind Hankel function of order one and with

$$\begin{aligned} a &= \left[\widetilde{v}_{i,\ell} - \widetilde{m}_j(s)\right]_1\,, \quad b = \left[\widetilde{v}_{i,\ell} - \widetilde{m}_j(s)\right]_2\,, \quad r = \sqrt{a^2+b^2}\,,\\ n_1 &= \left[\partial_s\widetilde{m}_j(s)\right]_2\,, \quad n_2 = -\left[\partial_s\widetilde{m}_j(s)\right]_1\,. \end{aligned}$$

Note that the Jacobian cancels out. A word has to be spent on the following issue: When $P \neq Q$ with $P = \widetilde{v}_{i,\ell}$ and $Q = \widetilde{m}_j(s)$, then the integrand of the integral of the right-hand side (9) is smooth. However, for the case $P = Q$ a singularity within the integral of the right-hand side (9) is present. In this case, we can use the singularity subtraction method to rewrite the singular integral in the following form

$$\begin{aligned} &\int_{\sigma} \partial_{v_1(\widetilde{m}_j(s))}\Phi_k(\widetilde{v}_{i,\ell},\widetilde{m}_j(s))\|\partial_s\widetilde{m}_j(s)\|\widetilde{L}_k(s)\,\mathrm{d}s(s)\\ &= \int_{\sigma} \partial_{v_1(\widetilde{m}_j(s))}\left(\Phi_k(\widetilde{v}_{i,\ell},\widetilde{m}_j(s)) - \Phi_0(\widetilde{v}_{i,\ell},\widetilde{m}_j(s))\right)\|\partial_s\widetilde{m}_j(s)\|\widetilde{L}_k(s)\,\mathrm{d}s(s)\\ &\quad + \int_{\sigma} \partial_{v_1(\widetilde{m}_j(s))}\Phi_0(\widetilde{v}_{i,\ell},\widetilde{m}_j(s))\|\partial_s\widetilde{m}_j(s)\|\widetilde{L}_k(s)\,\mathrm{d}s(s) = I_{i,\ell}^{\mathrm{smooth}} + I_{i,\ell}^{\mathrm{sing}} \end{aligned}$$

where $\Phi_0(P, Q) = -\log(|P-Q|)/(2\pi)$ is the fundamental solution of the Laplace equation. The integral $I_{i,\ell}^{\text{smooth}}$ has a smooth kernel (no singularity present) and is converging rapidly to zero when increasing the number of faces (independent of the wave number k). Hence, we directly set $I_{i,\ell}^{\text{smooth}} = 0$. The integral $I_{i,\ell}^{\text{sing}}$ (a singularity is present) can be rewritten as a sum of integrals without any singularity. This is due to the fact that we have $\mathrm{D}_0^{\Gamma_1 \to \Gamma_1}\psi(x) = -1/2$ with $\psi = 1, \forall x \in \Gamma_1$ (see [34, p. 363]) and hence, we approximately use for all i, ℓ:

$$\sum_{j=1}^{n_f}\sum_{k=1}^{3}\int_\sigma \partial_{\nu_1(\widetilde{m}_j(s))}\Phi_0(\widetilde{v}_{i,\ell}, \widetilde{m}_j(s))\|\partial_s\widetilde{m}_j(s)\|\widetilde{L}_k(s)\,\mathrm{d}s(s) \approx -\frac{1}{2}$$

(that is, the row sum of the matrix $\mathbf{M}(0)$ obtained from the discretization of the double layer for the Laplace equation shall be $-1/2$) and hence, we can compute $I_{i,\ell}^{\text{sing}}$ as

$$\begin{aligned} I_{i,\ell}^{\text{sing}} \approx\ & -\frac{1}{2} \\ & - \sum_{\substack{j=1 \\ (j,k)\neq(i,\ell)}}^{n_f}\sum_{k=1}^{3}\int_\sigma \partial_{\nu_1(\widetilde{m}_j(s))}\Phi_0(\widetilde{v}_{i,\ell}, \widetilde{m}_j(s))\|\partial_s\widetilde{m}_j(s)\|\widetilde{L}_k(s)\,\mathrm{d}s(s)\,. \end{aligned} \tag{10}$$

Each of the integrands within the integrals of the right-hand side (10) are smooth and can be computed with the previously mentioned Gauss-Kronrod quadrature.

Finally, if we use a domain with a hole, we obtain the system of size $m \times m = 2\cdot 3\cdot n_f \times 2\cdot 3\cdot n_f$ when including the boundary Γ_2 and the unknown function u_2. Written abstractly we obtain the non-linear eigenvalue problem

$$\mathbf{M}(k)u = 0 \tag{11}$$

Of course, the extension to more than one hole is obvious. In this case, the matrix $\mathbf{M}(k)$ within (11) will be of size $(q+1)\cdot 3\cdot n_f \times (q+1)\cdot 3\cdot n_f$ where q denotes the number of holes within the domain.

4.4 Non-linear eigenvalue problem

The non-linear eigenvalue problem (11) is solved with the Beyn algorithm [8]. It is based on complex-valued contour integrals integrating over the resolvent reducing the non-linear eigenvalue to a linear one (of very small size) which can be achieved by Keldysh's theorem. Precisely, a user-specified 2π-periodic contour γ of class C^1 within the complex plane has to be given. We need a contour that is enclosing a part of the real line where the smallest non-zero eigenvalue is expected. We usually use a circle with radius R and center $(\mu, 0)$ (in order to exclude the eigenvalue zero, we choose $\mu > R$). In this case, we have $\varphi(t) = \mu + R\cos(t) + \mathrm{i}R\sin(t)$ which satisfies $\varphi \in C^\infty$. The number of eigenvalues including their multiplicity within the

contour γ is denoted by $n(\gamma)$. With the randomly chosen matrix $\hat{\mathbf{V}} \in \mathbb{C}^{m\times\ell}$ with $m \gg \ell \geq n(\gamma)$ the two contour integrals of the form

$$\mathbf{A}_0 = \frac{1}{2\pi \mathrm{i}} \int_\gamma \mathbf{M}^{-1}(k)\hat{\mathbf{V}}\, \mathrm{d}s(k)\,,$$
$$\mathbf{A}_1 = \frac{1}{2\pi \mathrm{i}} \int_\gamma k\mathbf{M}^{-1}(k)\hat{\mathbf{V}}\, \mathrm{d}s(k)$$

over the given contour γ are now rewritten as

$$\mathbf{A}_0 = \frac{1}{2\pi \mathrm{i}} \int_0^{2\pi} \mathbf{M}^{-1}(\varphi(t))\hat{\mathbf{V}}\varphi'(t)\, \mathrm{d}s(t)\,,$$
$$\mathbf{A}_1 = \frac{1}{2\pi \mathrm{i}} \int_0^{2\pi} \varphi(t)\mathbf{M}^{-1}(\varphi(t))\hat{\mathbf{V}}\varphi'(t)\, \mathrm{d}s(t)$$

and approximated by the trapezoidal rule yielding

$$\mathbf{A}_{0,N} = \frac{1}{\mathrm{i}N} \sum_{j=0}^{N-1} \mathbf{M}^{-1}(\varphi(t_j))\hat{\mathbf{V}}\varphi'(t_j),$$
$$\mathbf{A}_{1,N} = \frac{1}{\mathrm{i}N} \sum_{j=0}^{N-1} \varphi(t_j)\mathbf{M}^{-1}(\varphi(t_j))\hat{\mathbf{V}}\varphi'(t_j)\,,$$

where the parameter N is given and the equidistant nodes are $t_j = 2\pi j/N$, $j = 0, \ldots, N$. Note that the choice $N = 24$ is usually sufficient, which is due to the exponential convergence rate ([8, Theorem 4.7]). The next step is the computation of a singular value decomposition of $\mathbf{A}_{0,N} = \mathbf{V}\Sigma\mathbf{W}^{\mathrm{H}}$ with $\mathbf{V} \in \mathbb{C}^{m\times\ell}$, $\Sigma \in \mathbb{C}^{\ell\times\ell}$, and $\mathbf{W} \in \mathbb{C}^{\ell\times\ell}$. Then, we perform a rank test for the matrix $\Sigma = \mathrm{diag}(\sigma_1, \sigma_2, \ldots, \sigma_\ell)$ for a given tolerance $\epsilon = \mathrm{tol}_{\mathrm{rank}}$ (usually $\epsilon = 10^{-4}$). That is, find $n(\gamma)$ such that $\sigma_1 \geq \ldots \geq \sigma_{n(\gamma)} > \epsilon > \sigma_{n(\gamma)+1} \geq \ldots \geq \sigma_\ell$. Define $\mathbf{V}_0 = (\mathbf{V}_{ij})_{1\leq i\leq m, 1\leq j\leq n(\gamma)}$, $\Sigma_0 = (\Sigma_{ij})_{1\leq i\leq n(\gamma), 1\leq j\leq n(\gamma)}$, and $\mathbf{W}_0 = (\mathbf{W}_{ij})_{1\leq i\leq \ell, 1\leq j\leq n(\gamma))}$ and compute the $n(\gamma)$ eigenvalues k_i and eigenvectors s_i of the matrix $\mathbf{B} = \mathbf{V}_0^{\mathrm{H}}\mathbf{A}_{1,N}\mathbf{W}_0\Sigma_0^{-1} \in \mathbb{C}^{n(\gamma)\times n(\gamma)}$. The ith non-linear eigenvector u_i is given by $\mathbf{V}_0 s_i$.

We refer the reader to [8, p. 3849] for more details on the implementation of this algorithm and the detailed analysis behind it including the proof of exponential convergence.

4.5 Eigenfunction

After we obtain the smallest non-zero eigenvalue k and the corresponding function u on the boundary from (11), we insert this into (3) to compute the eigenfunction inside the domain at any point we want. The discretization of the integrals is done as explained previously. Precisely, we have

$$u(x) = -\mathrm{DL}_k^{\Gamma_1} u_1(x) - \mathrm{DL}_k^{\Gamma_2} u_2(x) \approx -\sum_{j=1}^{n_f}\sum_{k=1}^{3} \left(\hat{a}_{j,k} u_1(\widetilde{v}_{j,k}) + \hat{b}_{j,k} u_2(\widetilde{v}_{j,k})\right)$$

with

$$\hat{a}_{j,k} = \int_\sigma \partial_{v_1(\widetilde{m}_j(s))} \Phi_k(x, \widetilde{m}_j(s)) \|\partial_s \widetilde{m}_j(s)\| \widetilde{L}_k(s) \, \mathrm{d}s(s)$$
$$\hat{b}_{j,k} = \int_\sigma \partial_{v_2(\widetilde{m}_j(s))} \Phi_k(x, \widetilde{m}_j(s)) \|\partial_s \widetilde{m}_j(s)\| \widetilde{L}_k(s) \, \mathrm{d}s(s)$$

for an arbitrary point $x \in D$. In fact, we can find maximal or minimal values by maximizing or minimizing this function. This is done by the Nelder-Mead algorithm (in Matlab by the fminsearch function), refer also to [25].

4.6 Superconvergence

The convergence of the method is out of the scope of this paper. Standard convergence results are available for boundary integral equations of the second kind using boundary element collocation method under suitable assumptions on the boundary (for example the boundary is at least of class C^2 to ensure compactness of the integral operator) and the boundary function for the Laplace equation (see [5, Section 9.2]). Quadratic approximations of the boundary and the boundary function yield cubic convergence (refer to [5, Theorem 9.2.1] for the Laplace equation and [21, Theorem 3.1] for the Helmholtz equation). In fact, the convergence results can be improved as shown in [5, Theorem 9.2.2] and [21, Theorem 4.10] for the three-dimensional case. However, the exact theoretical convergence rate for the eigenvalue is not known. It is expected that it is at least of order three, but we see later in the numerical results that it is better than three (for a sufficiently smooth boundary). Future work in this direction could be done using the ideas of Steinbach & Unger [38].

Finally, note that a specific choice of $0 < \alpha < 1/2$ can improve the overall convergence rate for smooth boundaries (see [21, p. 121 & p. 139]), but since we are happy with the cubic convergence rate with the pick $\alpha = (1 - \sqrt{3/5})/2$ (a Gauss-quadrature point within the interval [0, 1]), we have not investigated this any further.

5 Numerical results

5.1 Simply connected convex domains

First, we check the correctness and the convergence of the underlying method for the unit circle. It is known that the first non-trivial interior Neumann eigenvalue is the smallest positive root of J_1' (the first derivative of the first-kind Bessel function of order one). The root can be computed to arbitrary precision with Maple with the command

```
restart; Digits:=16: fsolve(diff(BesselJ(1,x),x),x=1..2);
```

It is approximately given by

$$1.841\,183\,781\,340\,659\,. \tag{12}$$

For the Beyn algorithm we use the parameters $N = 24$, $R = 1/2$, $\mu = 2$, and $\ell = 10$ for various number of faces n_f and number of collocation points

n_c. With the definition of the absolute error $E_{n_f}^{(i)}$ of the ith eigenvalue approximation, we compute the error of the first non-trivial eigenvalue $E_{n_f}^{(1)}$ of our method compared with (12). Additionally, we define the estimated order of convergence $\mathrm{EOC}^{(i)} = \log(E_{n_f}^{(i)}/E_{2\cdot n_f}^{(i)})/\log(2)$ of the ith eigenvalue approximation and compute $\mathrm{EOC}^{(1)}$. As we can see in Table 1, the first non-trivial Neumann eigenvalue can be made accurate up to eleven digits.

The estimated order of convergence is at least of order three. Note that we can go beyond eleven digits accuracy by further increasing n_f, but it is not necessary here.

Next, we show the influence of the algebraic multiplicity of the eigenvalue. The first non-trivial interior Neumann eigenvalue for the unit circle has algebraic multiplicity two. The same is true for the second non-trivial interior Neumann eigenvalue. It is obtained by computing the first positive root of J_2' approximately given by 3.054 236 928 227 140. The third non-trivial interior Neumann eigenvalue is simple and obtained by computing the second root of J_0' given by 3.831 705 970 207 512. Note that the first root of J_0' is zero which corresponds to the interior Neumann eigenvalue zero with a corresponding eigenfunction which is a constant. In Table 2, we show the absolute error and the estimated order of convergence for the second and third non-zero interior Neumann eigenvalue for a unit circle where we used different numbers of faces and different numbers of collocation points using the parameters $N = 24$, $R = 1/2$, $\mu = 3$, and $\ell = 10$.

Again, we notice the estimated order of convergence of at least order three and that we can achieve the order and the high accuracy regardless of the algebraic multiplicity of the eigenvalue.

We define $\square_\kappa = [-\kappa, \kappa] \times [-\kappa, \kappa]$ with $\kappa \in \mathbb{R}_{>0}$. In general, we use a resolution of 100×100 equidistantly distributed points, here within $\square_{1.1}$ and compute for each point that is located inside the unit circle the value of the eigenfunction. In Fig. 7, we show the eigenfunctions corresponding to the first three non-trivial interior Neumann eigenvalues as a contour plot with 40 contour lines. We also include the location of the maximum and minimum of the eigenfunction that corresponds to the first non-trivial interior Neumann eigenvalue as a red and blue dot, respectively.

Table 1 Absolute error and estimated order of convergence of the first non-trivial interior Neumann eigenvalue for a unit circle using different numbers of faces and collocation points

n_f	n_c	abs. error $E_{n_f}^{(1)}$	$\mathrm{EOC}^{(1)}$
5	15	5.8503_{-3}	
10	30	4.7818_{-4}	3.6129
20	60	4.5775_{-5}	3.3849
40	120	5.0168_{-6}	3.1897
80	240	5.9173_{-7}	3.0838
160	480	7.2096_{-8}	3.0369
320	960	8.9069_{-9}	3.0169
640	1920	1.1072_{-9}	3.0080
1280	3840	1.3803_{-10}	3.0039

Table 2 Absolute error and estimated order of convergence of the second and third non-trivial interior Neumann eigenvalue for a unit circle using different numbers of faces and collocation points

n_f	n_c	abs. error $E^{(2)}_{n_f}$	$\mathrm{EOC}^{(2)}$	abs. error $E^{(3)}_{n_f}$	$\mathrm{EOC}^{(3)}$
5	15	1.2817_{-2}		1.6335_{-2}	
10	30	1.1543_{-3}	3.4729	1.3081_{-3}	3.6424
20	60	1.2187_{-4}	3.2437	1.3133_{-4}	3.3162
40	120	1.4173_{-5}	3.1041	1.5147_{-5}	3.1161
80	240	1.7199_{-6}	3.0428	1.8416_{-6}	3.0401
160	480	2.1229_{-7}	3.0182	2.2788_{-7}	3.0146
320	960	2.6386_{-8}	3.0082	2.8373_{-8}	3.0057
640	1920	3.2895_{-9}	3.0038	3.5406_{-9}	3.0024
1280	3840	4.1066_{-10}	3.0018	4.4225_{-10}	3.0011

We can see that the extreme values for the first non-trivial interior Neumann eigenfunction of the unit circle are obtained on the boundary as it is conjectured for simply connected convex domains. Note that the second eigenfunction corresponding to the first non-trivial interior Neumann eigenvalue is a rotated version of the first eigenfunction.

We also show the eigenfunctions including the maximal and minimal value for a variety of other simply connected convex domains in Fig. 8 such as an ellipse and two deformed ellipses. The boundary of the ellipse is given in parametric form as $(6\cos(t)/5, \sin(t))^\top$ with $t \in [0, 2\pi)$. We use the parameters as before for Beyn's algorithm except $\mu = 1.5$ and consider $\square_{1.3}$. The first non-trivial interior Neumann eigenvalue is given by 1.544 422 which has algebraic multiplicity one. The parametrization of the deformed ellipse's boundary is given by $(0.75\cos(t) + \varepsilon\cos(2t), \sin(t))^\top$ with $t \in [0, 2\pi)$, where the parameter ε is chosen to be 0.1 and 0.2 (see [11, 23] for its first and second use). Using $n_f = 320$, the first non-trivial interior Neumann eigenvalue of the deformed ellipses with $\varepsilon = 0.1$ and $\varepsilon = 0.2$ are 1.849 064 and 1.819 478, respectively. Again, they both have algebraic multiplicity one.

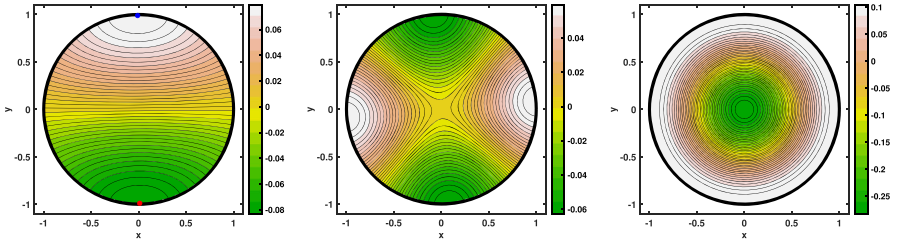

(a) First eigenfunction of a unit circle (b) Second eigenfunction of a unit circle (c) Third eigenfunction of a unit circle

Fig. 7 The first three eigenfunctions corresponding to the first three non-trivial interior Neumann eigenvalues 1.841 184, 3.054 237, and 3.831 706 for the unit circle

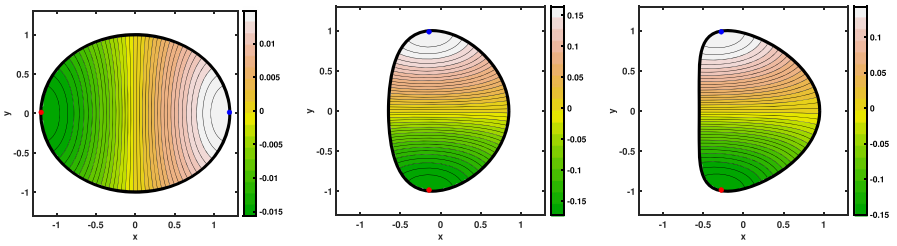

(a) First eigenfunction of an ellipse (b) First eigenfunction of a deformed ellipse with $\varepsilon = 0.1$ (c) First eigenfunction of a deformed ellipse with $\varepsilon = 0.2$

Fig. 8 The eigenfunctions corresponding to the first non-trivial interior Neumann eigenvalues for the ellipse and two deformed ellipses with $\varepsilon = 0.1$ and $\varepsilon = 0.2$ with corresponding non-trivial interior Neumann eigenvalue 1.544 422, 1.849 064, and 1.819 478

It is generally believed that the hot spots conjecture for general simply connected convex domains is true, but a general proof is still open. In all our numerical results for simply connected convex domains, we obtain the extrema on the boundary as one can see in Fig. 8.

5.2 Simply connected non-convex domains

No simply connected non-convex domain has yet been found (neither theoretically nor numerically) that fails the hot spots conjecture. Now, we concentrate on this case. We consider the deformed ellipse from the previous section with $\varepsilon = 0.3$, the peanut-shaped domain and the apple-shaped domain. The boundaries of the last two domains are given parametrically as $\sqrt{\cos^2(t) + \sin^2(t)/4}\,(\cos(t), \sin(t))^\top$ and $\frac{0.5+0.4\cos(t)+0.1\sin(2t)}{1+0.7\cos(t)}\,(\cos(t), \sin(t))^\top$ with $t \in [0, 2\pi)$, respectively (see [41] for its use). We use the parameters as before with $\mu = 1.5$ for the first two domains and $\mu = 3$ for the apple-shaped domain. Using $n_f = 320$, the first non-trivial interior Neumann eigenvalue for the three domains are 1.770 906, 1.721 292, and 2.761 274, respectively. They are all simple. As we can see in Fig. 9, the maximum and minimum are obtained on the boundary of the domains using $\square_{1.3}$.

Interesting domains have been constructed by Kleefeld (refer to [19] for more details) and extended by Abele and Kleefeld [1] for the purpose of finding new shape optimizers for certain non-trivial Neumann eigenvalues. The boundaries of the domains considered in those articles are given by 'generalized' equipotentials which are implicit curves. The simplest equipotential is of the form $\sum_{i=1}^{m} \|x - P_i\|^{-1} = c$ where the points $P_i \in \mathbb{R}^2$, $i = 1, \ldots, m$, the number of points m, and the parameter c are given. All $x \in \mathbb{R}^2$ that satisfy the equation describe the boundary of the domain. We use this idea to construct three non-symmetric and non-convex simply connected domains, say D_1, D_2, and D_3. For the boundary of the domain D_1, we use the parameter $m = 3$ and $c = 14/5$. The three points are $(-1, 1/2)^\top$, $(1, 1/3)^\top$, and $(0, 4/5)^\top$. Using $\mu = 1$, we obtain the first non-trivial interior Neumann eigenvalue 1.051 055. For the plot of the eigenfunction, we use $\square_{1.6}$. The boundary of the second domain is constructed through the use of $m = 4$ and $c = 7/2$ and the points are $(-5/4, 1/10)^\top$,

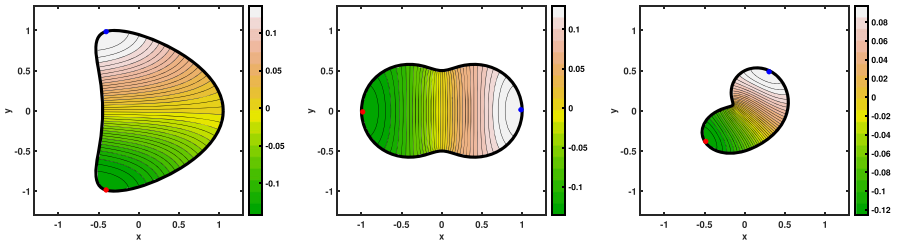

(a) First eigenfunction of a deformed ellipse with $\varepsilon = 0.3$ (b) First eigenfunction of a peanut (c) First eigenfunction of an apple

Fig. 9 The eigenfunctions corresponding to the first non-trivial interior Neumann eigenvalues for the deformed ellipse with $\varepsilon = 0.3$, the peanut-shaped, and the apple-shaped domain with corresponding non-trivial interior Neumann eigenvalue 1.770 906, 1.721 292, and 2.761 274

$(5/4, 0)^\top$, $(1/10, -1)^\top$, and $(0, 1)^\top$. We obtain the first non-trivial interior Neumann eigenvalue 1.086 037 when using $\mu = 1$ and the eigenfunction using $\square_{1.8}$. The third domain's boundary is constructed using $m = 5$ and $c = 18/5$ and the points are $(-1, 1/2)^\top$, $(1, 1/2)^\top$, $(0, -1)^\top$, $(3/2, -1)^\top$, and $(-3/2, -6/5)^\top$. Using $\mu = 1$, we obtain the first non-trivial interior Neumann eigenvalue 0.861 858. A plot of the corresponding eigenfunction is shown within $\square_{2.1}$.

All three eigenfunctions including the location of the maximal and minimal value are shown in Fig. 10.

As we can see again, the extreme values are obtained on the boundary.

In sum, we are not able to construct a simply connected non-convex domain that fails the hot spots conjecture. Next, we concentrate on non-simply connected domains.

5.3 Non-simply connected domains

Now, we consider an annulus with inner radius $R_1 = 1/2$ and outer radius $R_2 = 2$. For this domain, we can again compute a reference solution to arbitrary precision. The non-trivial interior Neumann eigenvalues are obtained through the roots of

$$J_n'(R_1 x)Y_n'(R_2 x) - J_n'(R_2 x)Y_n'(R_1 x) = 0\,, \quad n = 0, 1, 2, \ldots$$

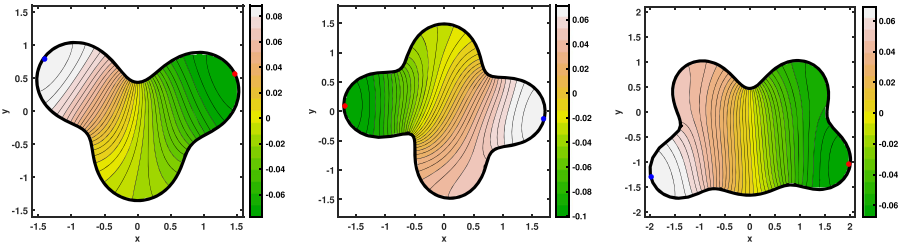

(a) First eigenfunction of D_1 (b) First eigenfunction of D_2 (c) First eigenfunction of D_3

Fig. 10 The eigenfunctions corresponding to the first non-trivial interior Neumann eigenvalues for domains D_1, D_2, and D_3 with corresponding non-trivial interior Neumann eigenvalue 1.051 055, 1.086 037, and 0.861 858

where Y_n' denotes the derivative of the second-kind Bessel function of order n. (see for example [40, Equation 4.16]). The first two roots are obtained with the Maple command

```
restart; Digits:=16:
Jp:=unapply(diff(BesselJ(1,x),x),x):
Yp:=unapply(diff(BesselY(1,x),x),x):
fsolve(Jp(x/2)*Yp(2*x)-Jp(2*x)*Yp(x/2),x=1);
Jp:=unapply(diff(BesselJ(2,x),x),x):
Yp:=unapply(diff(BesselY(2,x),x),x):
fsolve(Jp(x/2)*Yp(2*x)-Jp(2*x)*Yp(x/2),x=1);
```

The two smallest roots are approximately given by

$$0.822\,252\,688\,623\,884 \quad \text{and} \quad 1.504\,647\,782\,189\,479\,,$$

respectively. They both have multiplicity two. Again, we show in Table 3 that our method is able to achieve ten digits accuracy with a cubic convergence order for the first two non-trivial interior Neumann eigenvalues for an annulus using the parameter $\mu = 6/5$ for various number of faces. Note that twice the number of faces is needed due to the need of two boundary curves.

In Fig. 11 we show the first three eigenfunctions for $\square_{2,1}$ corresponding to the non-trivial interior Neumann eigenvalues 0.822 253, 1.504 648, and 2.096 773. To compute the third eigenvalue which has multiplicity two, we used $\mu = 2$. For the first eigenfunction plot, we also added the extreme values.

We can see that the extreme values are again obtained on the boundary of the annulus. Now, we consider more complex non-simply connected domains. The first domain A_1 is given by a unit circle centered at the origin removing an ellipse centered at $(-0.5, -0.3)^\top$ with semi-axis 0.15 and 0.35. We obtain the first non-trivial interior Neumann eigenvalue 1.662 873 and the eigenfunction within $\square_{1,1}$. The second domain A_2 is given by D_3 removing an ellipse centered at $(-0.1, -0.3)^\top$ with semi-axis 0.15 and 0.35. We get the first non-trivial interior Neumann eigenvalue 1.651 571 and the eigenfunction within $\square_{1,1}$. The third domain A_3 is given by D_3 removing a 90 degree counter-clockwise rotated version of D_3 scaled by $1/2$. We obtain the

Table 3 Absolute error and estimated order of convergence of the first and second non-trivial interior Neumann eigenvalue for an annulus with $R_1 = 1/2$ and $R_2 = 2$ using different numbers of faces and collocation points

$2n_f$	$2n_c$	Absolute error $E_{n_f}^{(1)}$	$\text{EOC}^{(1)}$	Absolute error $E_{n_f}^{(2)}$	$\text{EOC}^{(2)}$
10	30	2.4700_{-3}		6.1268_{-3}	
20	60	1.9490_{-4}	3.6637	5.4708_{-4}	3.4853
40	120	1.7741_{-5}	3.4575	5.7347_{-5}	3.2540
80	240	1.8725_{-6}	3.2441	6.6443_{-6}	3.1095
160	480	2.1655_{-7}	3.1122	8.0539_{-7}	3.0443
320	960	2.6159_{-8}	3.0493	9.9900_{-8}	3.0111
640	1920	3.2351_{-9}	3.0154	1.2988_{-8}	2.9433

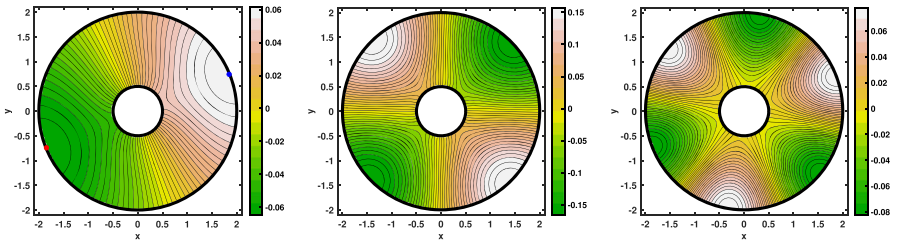

(a) First eigenfunction of an annulus (b) Second eigenfunction of an annulus (c) Third eigenfunction of an annulus

Fig. 11 The first three eigenfunctions corresponding to the first three non-trivial interior Neumann eigenvalues 0.822 253, 1.504 648, and 2.096 773 for an annulus

first non-trivial interior Neumann eigenvalue 1.171 590 and the eigenfunction within $\square_{1.1}$. We used the parameter $\mu = 1.5$ for all three domains. The eigenfunctions for A_1, A_2, and A_3 including the extreme values are illustrated in Fig. 12.

As we can see again, the extreme values are obtained on the boundary. We also tried many other similar geometries with different kinds of holes and obtained similar results. The hot spots conjecture seems to hold.

Finally, we concentrate on a more complex geometry inspired by the work of Burdzy [9, Figure 1] as shown in Fig. 13. We shortly explain how he constructed the domain D with one hole that does not satisfy the hot spots conjecture. For simplicity, we illustrate only the construction of a quarter of the domain, say $D_{1/4}$. Let $\varepsilon \in (0, 1/4)$ and $\varepsilon_0 \in (0, \varepsilon)$. Define the points $(0, -\varepsilon)^\top$, $(1, 2\varepsilon)^\top$, $(2, \varepsilon_0)^\top$, $(2, -\varepsilon_0)^\top$, $(1, -2\varepsilon)^\top$, and $(0, -\varepsilon)^\top$. Next, construct the convex polygon A_1 with those points. Now, define the polygonal Jordan arc C_1 lying inside the domain

$$\Big(B((2,-1)^\top, 1+2\varepsilon_0) \backslash B((2,-1)^\top, 1+\varepsilon_0/2)\Big) \cap \{(x,y)^\top : x \geq 2\,, y \geq -1\}$$

with endpoints $(2, \varepsilon_0)^\top$ and $(3+\varepsilon_0, -1)^\top$ where $B((x_0, y_0)^\top, r)$ denotes the open disk centered at the location $(x_0, y_0)^\top$ and radius r satisfying for any line segment $\overline{x, y}, \overline{y, z} \subset C_1$ the condition $|\angle(y-x, z-y)| \leq \varepsilon_0$. Likewise, the polygonal Jordan

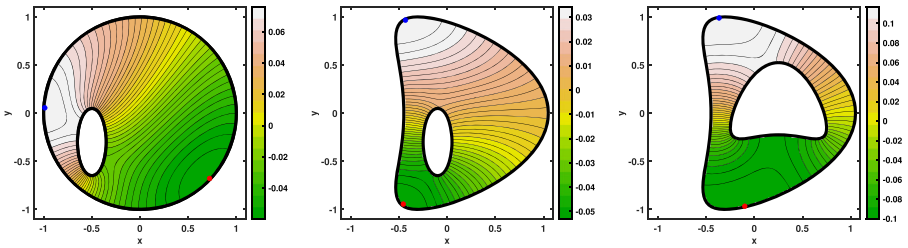

(a) First eigenfunction of A_1 (b) First eigenfunction of A_2 (c) First eigenfunction of A_3

Fig. 12 The eigenfunctions corresponding to the first non-trivial interior Neumann eigenvalues 1.662 873, 1.651 571, and 1.171 590 for the domains A_1, A_2, and A_3

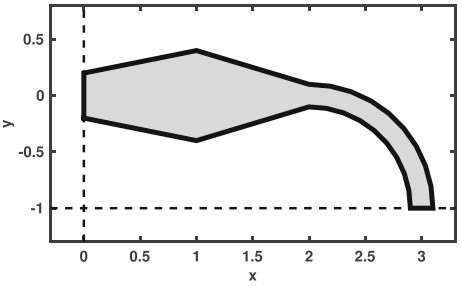

Fig. 13 A quarter of the domain constructed by Burdzy [9, Figure 1] using the parameters $\varepsilon = 0.2$ and $\varepsilon_0 = 0.1$

arc C_2 is defined inside

$$\Big(B((2,-1)^\top, 1-\varepsilon_0/2)\backslash B((2,-1)^\top, 1-2\varepsilon_0)\Big) \cap \{(x,y)^\top \,:\, x \geq 2\,, y \geq -1\}$$

with endpoints $(2, -\varepsilon_0)^\top$ and $(3-\varepsilon_0, -1)^\top$. The boundary of the domain A_2 is given by C_1, C_2, and the two line segments connecting the two points $(2, \varepsilon_0)^\top$ and $(2, -\varepsilon_0)^\top$ and the two points $(3+\varepsilon_0, -1)^\top$, $(3-\varepsilon_0, -1)^\top$, respectively. The complete domain D is now obtained by mirroring $D_{1/4} = A_1 \cup A_2$ along the y-axis ($x = 0$) followed by mirroring along $y = -1$.

Our method cannot be applied to this domain due to three reasons: The domain is of polygonal structure, it contains polygonal Jordan arcs satisfying certain angular conditions, and it is very thin.

Therefore, we construct less complex domains (inspired by Burdzy's domain) that fail the hot spots conjecture and numerically show the failure. Further, we show the exact location of the extreme values.

The 'teether' domain depicted in Fig. 14 is constructed as follows:

Let $E(x, y, a, b, t_1, t_2)$ be the ellipse centered at $(x, y)^\top$ with semi-axis a and b constructed for $\phi \in [t_1, t_2)$ using the parametrization $(x + a\cos(\phi), y + b\sin(\phi))^\top$. Note that we also allow $t_1 > t_2$ to guarantee the needed orientation of the curve. The first half of the outer boundary is given by the pieces $E(4, 4, 1, 1, -$

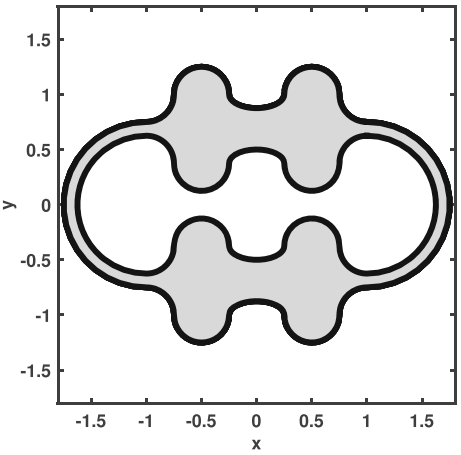

Fig. 14 A more advanced bounded domain with a hole inspired by the work of Burdzy [9, Figure 1]

$\pi/2, -\pi)$, $E(2, 4, 1, 1, 0, \pi)$, $E(0, 4, 1, 1/2, 0, -\pi)$, $E(-2, 4, 1, 1, 0, \pi)$, $E(-4, 4, 1, 1, 0, -\pi/2)$, and $E(-4, 0, 3, 3, \pi/2, 3\pi/2)$. Rotating this half by π yields the second half of the outer boundary. The first half of the inner boundary is given by the pieces $E(4, 3/2, 1, 1, \pi/2, \pi)$, $E(2, 3/2, 1, 1, 0, -\pi)$, $E(0, 3/2, 1, 1/2, 0, \pi)$, $E(-2, 3/2, 1, 1, 0, -\pi)$, $E(-4, 3/2, 1, 1, 0, \pi/2)$, and $E(-4, 0, 5/2, 5/2, \pi/2, 3\pi/2)$. Rotating this half by π yields the second half of the inner boundary. Next, the orientation of the inner boundary is reversed. Finally, all coordinates of the boundary are multiplied with $1/4$. This yields our 'teether' domain C_1.

We use the parameter $\mu = 0.8$, $\ell = 20$ and $\square_{1.8}$. We obtain the first non-trivial interior Neumann eigenvalue 0.370 708. The corresponding eigenfunction including is extreme values is shown in Fig. 15. Since the extreme values lie in very flat plateaus, we additionally show zoomed versions around the extreme values to better see that they are located inside the domain.

This shows that we are able to show numerically that there exists a bounded domain with one hole that fails the hot spots conjecture.

Next, we investigate some possible conditions needed to construct an example that fails the hot spots conjecture. With one bump it was not possible to obtain the extreme values inside the domain, say C_2. We use the previous example, and remove one of the bump and its mirror version in the upper and lower part of the teether domain. We obtain the first non-trivial interior Neumann eigenvalue 0.534 605 and the corresponding eigenfunction within $\square_{1.6}$.

As we can see again in Fig. 16, the values inside the bump area are very close to each other. The extreme values are attained on the boundary.

Right now, the proposed domain C_1 has two lines of symmetry as the domain by Burdzy does. Now, we break the symmetry and show that we are still able to obtain a counter-example of the hot spots conjecture. We add a small amount of $\rho = 0.0250$ to the semi-axis of the ellipse that describes the upper left bump and obtain the domain C_3. The first non-trivial interior Neumann eigenvalue is 0.370 054.

As we can see in Fig. 17, the location of the hot spots of the eigenfunction within $\square_{1.8}$ are slightly changed, too, but they remain inside of C_3. Increasing the value from $\rho = 0.025$ to $\rho = 0.125$ will shift the maximal value from inside the domain $\widetilde{C}_3$ to the boundary while the minimum stays inside the domain. We obtain the eigenvalue 0.367 496. The question remains for which parameter ρ between 0.025 and 0.125

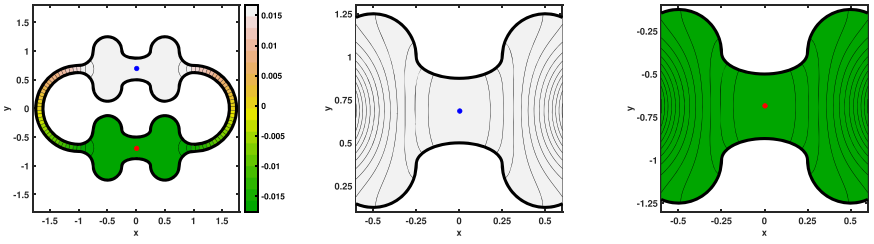

(a) First eigenfunction of C_1 (b) Zoom around the maximum (c) Zoom around the minimum

Fig. 15 The eigenfunction and its zoomed version around the maximum and minimum corresponding to the first non-trivial interior Neumann eigenvalue 0.370 708 for the teether domain C_1

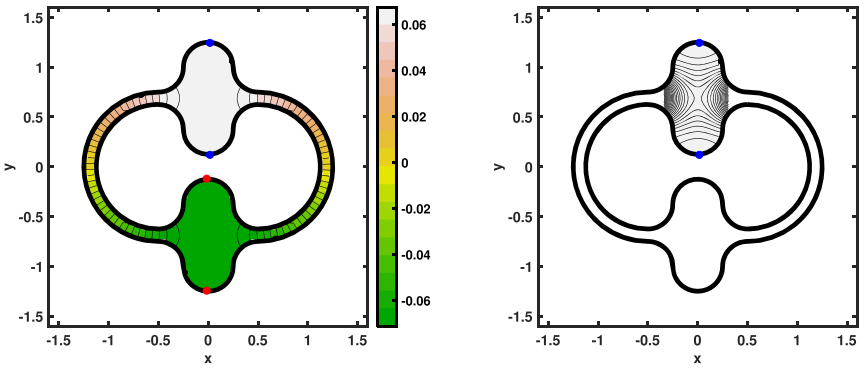

(a) First eigenfunction of C_2 (b) Zoom around the maximum

Fig. 16 The eigenfunction and its zoomed version around the maximum corresponding to the first non-trivial interior Neumann eigenvalue 0.534 605 for the domain C_2

will there be the change from the failure of the hot spots conjecture to its validity. The answer is reported in Table 4.

The switch between failure and validity is obtain for ρ between 0.1 and 0.1125.

We also show in Fig. 18 that the hot spots conjecture is true when we cut the upper middle connector of the teether domain C_1. Precisely, the width of the cut is approximately 0.049. The maximum and minimum are located at the centers of the cutting lines, respectively.

Now, we show what happens if we make the gap between $E(0, 4, 1, 1/2, 0, -\pi)$ and $E(0, 3/2, 1, 1/2, 0, \pi)$ and its mirror counterpart smaller. We use $E(0, 4, 1, 1, 0, -\pi)$ and $E(0, 3/2, 1, 1, 0, \pi)$ instead to obtain C_4. We obtain the first non-trivial interior Neumann eigenvalue 0.384 715 and its corresponding eigenfunction within $\square_{1.8}$ shown in Fig. 19.

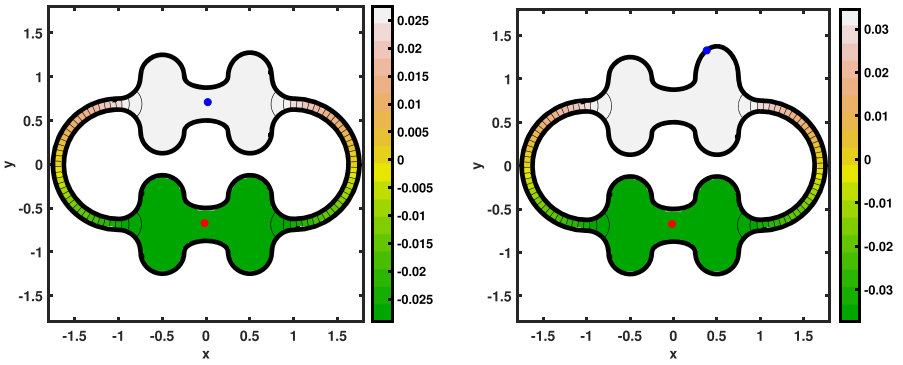

(a) First eigenfunction of C_3 (b) First eigenfunction of $\widetilde{C}_3$

Fig. 17 The eigenfunction corresponding to the first non-trivial interior Neumann eigenvalue 0.370 054 and 0.367 496 for the domains C_3 and $\widetilde{C}_3$

Table 4 The eigenvalue and failure depending on the parameter ρ for variants of C_1

ρ	Eigenvalue	Failure of HSC
0.0125	0.370 379	yes
0.0250	0.370 054	yes
0.0375	0.369 730	yes
0.0500	0.369 407	yes
0.0625	0.369 086	yes
0.0750	0.368 765	yes
0.0875	0.368 446	yes
0.1000	0.368 128	yes
0.1125	0.367 812	no
0.1250	0.367 496	no

Again the hot spots conjecture fails. Therefore, this example is interesting since Burdzy's original domain needs the assumption that the gap of the right pipe (the parameter ε_0) needs to be smaller than the gap between the bumps (the parameter ε).

Next, we show what happens if we make the bumps of the domain C_4 smaller. We construct the domain as before except that we introduce a new parameter $\delta > 0$. The first half of the outer boundary is given by the pieces $E(4, 3+\delta, 1, \delta, -\pi/2, -\pi)$, $E(2, 3+\delta, 1, \delta, 0, \pi)$, $E(0, 3+\delta, 1, \delta, 0, -\pi)$, $E(-2, 3+\delta, 1, \delta, 0, \pi)$, $E(-4, 3+\delta, 1, \delta, 0, -\pi/2)$, and $E(-4, 0, 3, 3, \pi/2, 3\pi/2)$. Rotating this half by π yields the second half of the outer boundary. The first half of the inner boundary is given by the pieces $E(4, 5/2-\delta, 1, \delta, \pi/2, \pi)$, $E(2, 5/2-\delta, 1, \delta, 0, -\pi)$, $E(0, 5/2-\delta, 1, \delta, 0, \pi)$, $E(-2, 5/2-\delta, 1, \delta, 0, -\pi)$, $E(-4, 5/2-\delta, 1, \delta, 0, \pi/2)$, and $E(-4, 0, 5/2, 5/2, \pi/2, 3\pi/2)$. Rotating this half by π yields the second half of the inner boundary. Next, the orientation of the inner boundary is reversed. Finally, all coordinates of the boundary are multiplied with $1/4$. Note that $\delta = 1$ yields the domain C_4.

We obtain the following results within $\square_{1.8}$ shown in Fig. 20 for $\delta = 1/4$, $\delta = 1/10$, and $\delta = 1/20$.

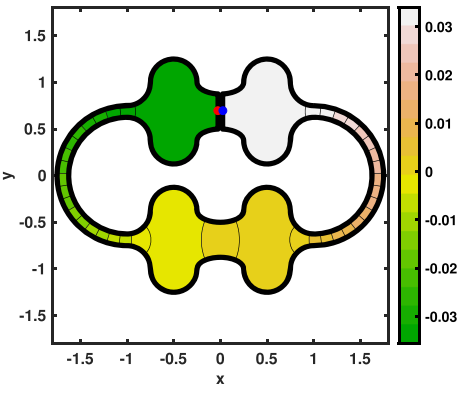

Fig. 18 The eigenfunction corresponding to the first non-trivial interior Neumann eigenvalue 0.246 286 for the teether domain C_1 cutting the upper middle connector

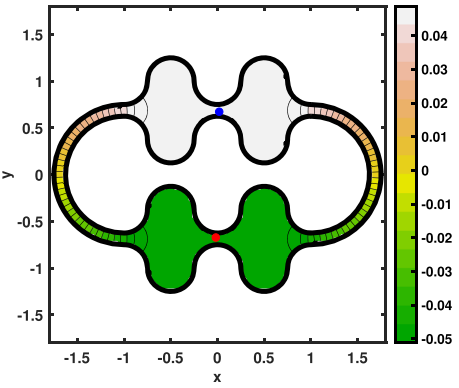

(a) First eigenfunction of C_4

Fig. 19 The eigenfunction corresponding to the first non-trivial interior Neumann eigenvalue 0.384 715 for the domains C_4

Surprisingly, the extreme values stay inside of the domain $\tilde{C}_4$, $\hat{C}_4$, and $\bar{C}_4$. Also note that the first non-trivial interior Neumann eigenvalue changes drastically.

Interestingly, we can also remove the bumps in the lower part of the teether domain C_1 and still obtain the extreme values inside the new domain C_5. The result is shown in Fig. 21 within $\square_{1.8}$. The corresponding non-trivial interior Neumann eigenvalue is 0.563 329.

The idea to also remove the bumps on the upper part yields the following results for the new 'stadium' domain S as shown in Fig. 22 within $\square_{1.8}$.

Unfortunately, the extreme values are now on the boundary of S. The first non-trivial interior Neumann eigenvalues is 0.755 416. The second non-trivial eigenvalue is very close (but distinct) 0.756 082. We can see that the limiting process of making the bumps of C_4 smaller (see also $\tilde{C}_4$ and $\hat{C}_4$) yields the eigenfunction corresponding to the second non-trivial interior Neumann eigenfunction for the domain S. This is very unexpected.

Further, it seems that the heat flow out of the narrow part of the 'pipes' has to be almost without inclination. We use the parametrization $r_i(t) \cdot (\sin(t), \cos(t))^\top$ with $r_i(t) = a_i(1 + 1/2 \sin(\omega t \cdot \mathbb{I}_{[(\omega/2-1)\pi/\omega,(\omega/2+1)\pi/\omega]\cup[(3\omega/2-1)\pi/\omega,(3\omega/2+1)\pi/\omega]}))$, $t \in$

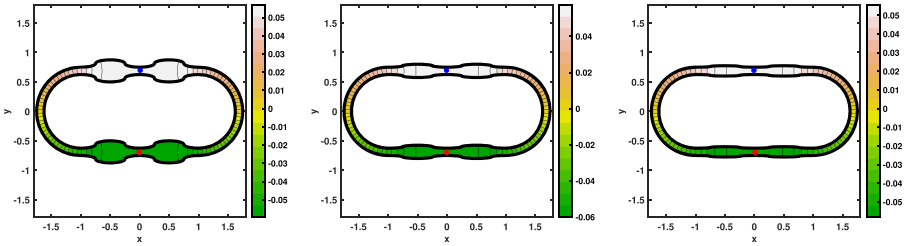

(a) First eigenfunction of $\tilde{C}_4$ (b) First eigenfunction of $\hat{C}_4$ (c) First eigenfunction of $\bar{C}_4$

Fig. 20 The eigenfunction corresponding to the first non-trivial interior Neumann eigenvalue 0.578 402, 0.668 373, and 0.708 633 for the domains $\tilde{C}_4$, $\hat{C}_4$ and $\bar{C}_4$, respectively

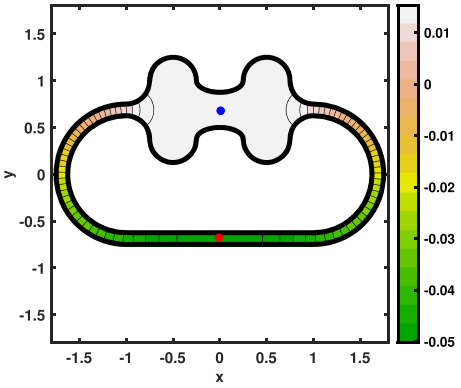

(a) First eigenfunction of C_5

Fig. 21 The eigenfunction corresponding to the first non-trivial interior Neumann eigenvalue 0.563 329 for the domain C_5

$[0, 2\pi)$ with $a_1 = 1$ for the outer boundary and $a_2 = 0.9$ for the inner boundary. Here $\mathbb{I}$ denotes the indicator function. We use $\omega = 4$ and $\omega = 8$ to construct the domains F_1 and F_2. We obtain the first non-trivial interior Neumann eigenvalue 1.592 787 and 1.717 098 and the eigenfunction within $\square_{1.6}$. As we can see in Fig. 23 the maximum and minimum value are obtained on the boundary. In fact, we have two maxima and two minima.

Next, we show in Table 5 for the different examples that show a failure of the hot spots conjecture the following information: The domain under consideration, the location of the global maximum and minimum inside the domain, and the ratio $\aleph_{max}$ and $\aleph_{min}$ which are defined as the ratio of the maximum inside the domain divided by the maximum on the boundary and likewise for the minimum. All ratios will be larger than one, but we are interested in how close they are to one. Recall that the hot spots conjecture fails if we have $\aleph_{max} > 1$ and/or $\aleph_{min} > 1$. The maximum and minimum are calculated through the Matlab minimization routine fminsearch by

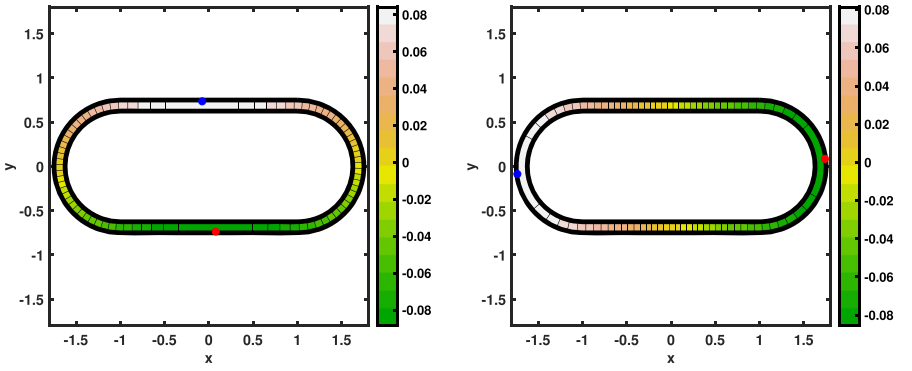

(a) First eigenfunction of S (b) Second eigenfunction of S

Fig. 22 The eigenfunctions corresponding to the first and second non-trivial interior Neumann eigenvalue 0.755 416 and 0.756 082 for the domain S

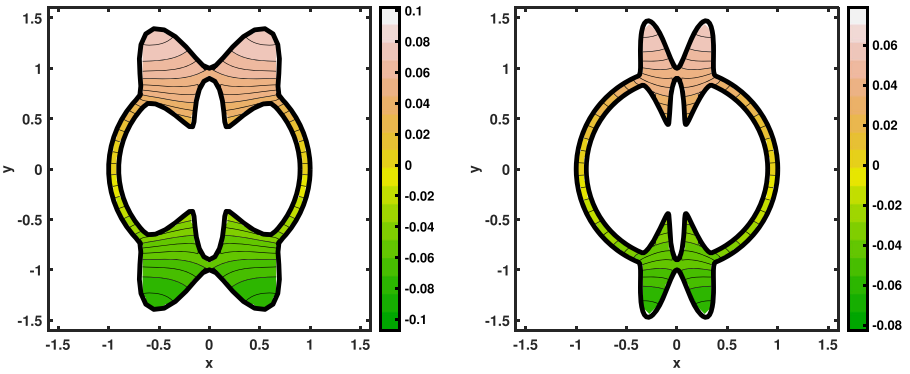

(a) First eigenfunction of F_1 (b) First eigenfunction of F_2

Fig. 23 The eigenfunction corresponding to the first non-trivial interior Neumann eigenvalue 1.592 787 and 1.717 098 for the domains F_1 and F_2, respectively

passing the function given in (2) to a tolerance of 10^{-10} for the step size and the difference of a function evaluation. For the first two domains, we use as starting value $(0, 0.6)^\top$ and $(0, -0.6)^\top$, respectively. For the next three domains, we use $(0, 0.69)^\top$ and $(0, -0.69)^\top$ and for the last domain, we use $(0, 0.6875)^\top$ and $(0, -0.6875)^\top$.

As we can see the maximum and minimum are approximately located on the y-axis each centered between the bumps for the first four domains. Interestingly, we obtain for the ratios $1 + \epsilon$ with very small $\epsilon > 0$. The parameter ϵ decreases as the shape gets closer to the 'stadium' domain. Hence, we might conjecture that there exists a domain with one hole where we have $\aleph_{max} = 1 + \epsilon$ and $\aleph_{min} = 1 + \epsilon$ with $\epsilon \geq \epsilon_0 > 0$ given ϵ_0 arbitrarily small. For the last domain, we obtain the largest value for ϵ. Precisely, we obtain $\epsilon_0 > 1 + 10^{-3}$. However, the location of the minimum might be on the boundary (or on the complete part of the y-axis).

How can we trust the errors that are presented in Table 5? We could numerically compute the location of the maximum and minimum as well as the ratios for three

Table 5 Location of the maximum and minimum inside the domain along with the ratios $\aleph_{max} > 1$ and/or $\aleph_{min} > 1$ for various domains D that fail the hot spots conjecture

D	Location max	Location min	$\aleph_{max}$	$\aleph_{min}$
C_1	$(-3.805_{-8}, 6.877_{-1})^\top$	$(3.299_{-8}, -6.877_{-1})^\top$	$1 + 1.221_{-4}$	$1 + 1.221_{-4}$
C_4	$(8.126_{-8}, 6.875_{-1})^\top$	$(-3.893_{-8}, -6.875_{-1})^\top$	$1 + 1.196_{-5}$	$1 + 1.196_{-5}$
$\tilde{C}_4$	$(-2.998_{-8}, 6.875_{-1})^\top$	$(-2.028_{-8}, -6.875_{-1})^\top$	$1 + 7.130_{-6}$	$1 + 7.118_{-6}$
$\hat{C}_4$	$(3.530_{-8}, 6.875_{-1})^\top$	$(2.824_{-8}, -6.875_{-1})^\top$	$1 + 3.808_{-6}$	$1 + 3.802_{-6}$
$\bar{C}_4$	$(-4.580_{-8}, 6.875_{-1})^\top$	$(-4.787_{-8}, -6.875_{-1})^\top$	$1 + 2.137_{-6}$	$1 + 2.138_{-6}$
C_5	$(-1.968_{-7}, 6.877_{-1})^\top$	————	$1 + 1.438_{-3}$	————

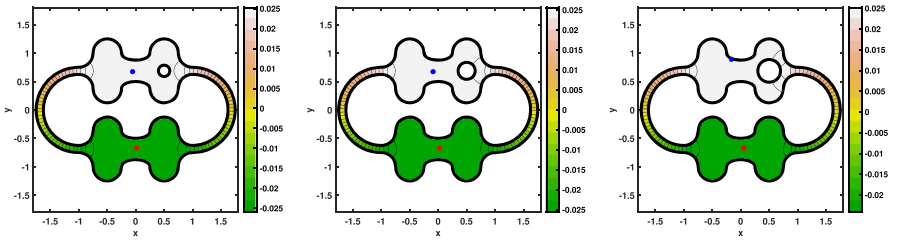

(a) First eigenfunction of $C_{1,0.1}$ (b) First eigenfunction of $C_{1,0.15}$ (c) First eigenfunction of $C_{1,0.2}$

Fig. 24 The eigenfunction corresponding to the first non-trivial interior Neumann eigenvalue 0.372 580, 0.374 917, and 0.378 131 for the domains $C_{1,0.1}$, $C_{1,0.15}$ and $C_{1,0.2}$, respectively

different numbers of collocation nodes and compute the estimated order of convergence by $\log(|u_{n_f} - u_{2n_f}|/|u_{2n_f} - u_{4n_f}|)/\log(2)$ (we do not know the exact solution as we did for Tables 1, 2, and 3), but this is very time consuming and not necessary here. We claim that the x-coordinate of the location of the maximum and minimum is zero due to the symmetry of all six domains considered in Table 5 which might be proven similarly with the techniques given in Burdzy [9]. Then, the results for the x-coordinate are accurate to eight digits. We claim the same is true for the y-coordinate and then as well as for the ratios.

5.4 Domains with more than one hole

Finally, we show without further discussion that we are also able to construct examples with more than one hole where the hot spots conjecture fails to hold. Using the teether domain C_1 and removing a circle centered at $(1/2, 11/16)^\top$ with radius $\mathfrak{R}$, yields a domain with two holes, say $C_{1,\mathfrak{R}}$. Using $\mathfrak{R} = 0.1$, $\mathfrak{R} = 0.15$, and $\mathfrak{R} = 0.2$, gives the results shown in Fig. 24 where we used the same set of parameters as for the results for C_1.

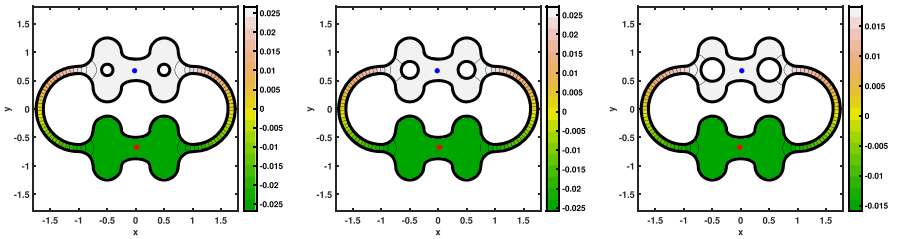

(a) First eigenfunction of $\widetilde{C}_{1,0.1}$ (b) First eigenfunction of $\widetilde{C}_{1,0.15}$ (c) First eigenfunction of $\widetilde{C}_{1,0.2}$

Fig. 25 The eigenfunction corresponding to the first non-trivial interior Neumann eigenvalue 0.374 552, 0.379 670, and 0.387 461 for the domains $\widetilde{C}_{1,0.1}$, $\widetilde{C}_{1,0.15}$ and $\widetilde{C}_{1,0.2}$, respectively

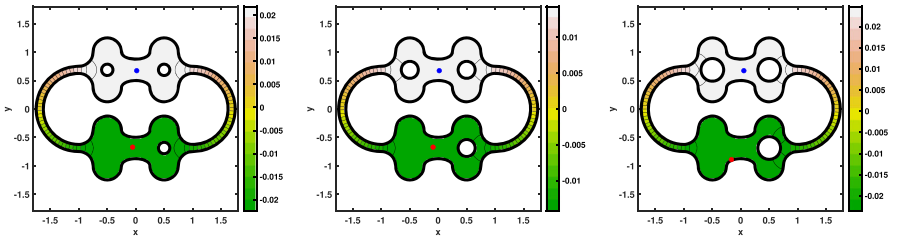

(a) First eigenfunction of $C^{\mathrm{mir}}_{1,0.1}$ (b) First eigenfunction of $C^{\mathrm{mir}}_{1,0.15}$ (c) First eigenfunction of $C^{\mathrm{mir}}_{1,0.2}$

Fig. 26 The eigenfunction corresponding to the first non-trivial interior Neumann eigenvalue 0.376 406, 0.383 781, and 0.394 522 for the domains $C^{\mathrm{mir}}_{1,0.1}$, $C^{\mathrm{mir}}_{1,0.15}$ and $C^{\mathrm{mir}}_{1,0.2}$, respectively

As we can see, the maximum and minimum still remain inside the domains $C_{1,0.1}$ and $C_{1,0.15}$. The location of the maximum is slightly shifted to the right whereas the minimum is slightly shifted to the left for the first two cases. If the radius of the removed circle is large, then the maximum goes to the boundary whereas the minimum stays inside the domain $C_{1,0.2}$ as shown in the last contour plot of Fig. 24. Next, we construct domains with three holes. Therefore, we use the previous domain $C_{1,\mathfrak{R}}$ and mirror the circular hole at the y-axis. This yields the domain $\widetilde{C}_{1,\mathfrak{R}}$. Using the same parameters as before yields the results shown in Fig. 25.

As we can see now, the maximum and minimum remain inside all the three domains $\widetilde{C}_{1,0.1}$, $\widetilde{C}_{1,0.15}$, and $\widetilde{C}_{1,0.2}$. Next, we consider domains with four holes. Therefore, we use the domains $C_{1,0.1}$, $C_{1,0.15}$ and $C_{1,0.2}$ and mirror the upper right circular hole at the x-axis. This yields the domains $C^{\mathrm{mir}}_{1,0.1}$, $C^{\mathrm{mir}}_{1,0.15}$ and $C^{\mathrm{mir}}_{1,0.2}$, respectively. The results are presented in Fig. 26.

As expected, we obtain the minimal and maximal value inside the domain for the two domains $\widetilde{C}^{\mathrm{mir}}_{1,0.1}$ and $\widetilde{C}^{\mathrm{mir}}_{1,0.15}$ whereas the maximum is on the boundary for the domain $\widetilde{C}^{\mathrm{mir}}_{1,0.2}$. The domains with five holes $\widetilde{C}^{\mathrm{mir}}_{1,0.1}$, $\widetilde{C}^{\mathrm{mir}}_{1,0.15}$ and $\widetilde{C}^{\mathrm{mir}}_{1,0.2}$ are constructed by mirroring the domains $\widetilde{C}_{1,0.1}$, $\widetilde{C}_{1,0.15}$ and $\widetilde{C}_{1,0.2}$ at the x-axis. The results are shown in Fig. 27.

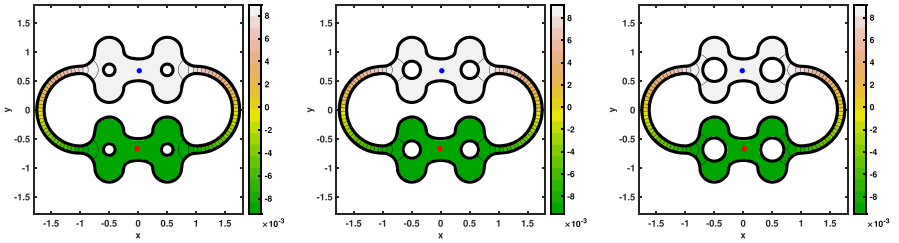

(a) First eigenfunction of $\widetilde{C}^{\mathrm{mir}}_{1,0.1}$ (b) First eigenfunction of $\widetilde{C}^{\mathrm{mir}}_{1,0.15}$ (c) First eigenfunction of $\widetilde{C}^{\mathrm{mir}}_{1,0.2}$

Fig. 27 The eigenfunction corresponding to the first non-trivial interior Neumann eigenvalue 0.378 360, 0.388 438, and 0.403 504 for the domains $\widetilde{C}^{\mathrm{mir}}_{1,0.1}$, $\widetilde{C}^{\mathrm{mir}}_{1,0.15}$ and $\widetilde{C}^{\mathrm{mir}}_{1,0.2}$, respectively

As we can see, the maximal and minimal values are attained inside all the considered domains with five holes.

The extension for the construction of domains having more than five holes which do not satisfy the hot spots conjecture is now straightforward.

6 Summary, conclusion, and outlook

In this paper, a detailed description is given on how to compute the first non-trivial eigenvalue and its corresponding eigenfunction for the Laplace equation with Neumann boundary condition for a given domain with one hole. The problem is reformulated as a non-linear eigenvalue problem involving boundary integral equations thus reducing a two-dimensional problem to a one-dimensional problem. Due to superconvergence we are able to achieve highly accurate approximations both for the eigenvalue and the eigenfunction. With this method at hand, we can compute the eigenvalue and eigenfunction for several different constructed domains. This gives the possibility to find domains with one hole failing the hot spots conjecture and investigate the influence of varying the domain. Some interesting observation can be made such as that the ratio between the maximal/minimal value inside the domain and the maximal/minimal value on the boundary can be $1 + 10^{-3}$. But the question remains whether there is an upper bound on this constant.

We conclude that simple domains can be constructed that fail the hot spots conjecture. Moreover, we conjecture that symmetry is not needed to construct domains that fail the hot spots conjecture as it was assumed for Burdzy's domain. However, a large deviation from symmetry shows that the hot spots conjecture is true. Hence, there is a certain switch between those two cases. Further, the gap size between the right pipe and the gap size between the two bumps can be the same. In Burdzy's domain the gap size of the pipe was assumed to be smaller. We conjecture that this assumption can be removed. Additionally, the flow outside the pipe needs to be horizontal. Using only a small deviation of the outflow of the pipe show that the hot spots conjecture holds. We conjecture that this is needed for the failure of the hot spots conjecture.

The Matlab codes including the produced data are available at github

https://github.com/kleefeld80/hotspots

and researchers can run it on their own constructed domains and reproduce the numerical results within this article. This might give new ideas whether one can find assumptions in order to prove or disprove the hot spots conjecture. The extension for domains with more than one hole is straightforward. For the sake of completeness they are given at the end of the numerical results section for domains with up to five holes, but without detailed discussion.

It would be interesting to check whether it is possible to construct three-dimensional domains with one hole that fail the hot spots conjecture, too. The software for a domain without a hole would already be available and only needs to be extended (see [18, 21] or other sophisticated software such as BEM++ [37]). The consideration of other partial differential equations in two or three dimensions whose fundamental solution is known together with Neumann boundary condition could be numerically investigated as well.

Acknowledgements The author thanks Prof. Stefan Steinerberger from the University of Washington, Seattle (USA) for the fruitful discussions during the preparation of the manuscript. Further, the author greatly acknowledges the referee's useful suggestions that considerably improved the initial version of the manuscript.

Funding Open Access funding enabled and organized by Projekt DEAL.

Declarations

Conflict of interest The author declares no conflict interests.

Open Access This article is licensed under a Creative Commons Attribution 4.0 International License, which permits use, sharing, adaptation, distribution and reproduction in any medium or format, as long as you give appropriate credit to the original author(s) and the source, provide a link to the Creative Commons licence, and indicate if changes were made. The images or other third party material in this article are included in the article's Creative Commons licence, unless indicated otherwise in a credit line to the material. If material is not included in the article's Creative Commons licence and your intended use is not permitted by statutory regulation or exceeds the permitted use, you will need to obtain permission directly from the copyright holder. To view a copy of this licence, visit http://creativecommons.org/licenses/by/4.0/.

References

1. Abele, D., Kleefeld, A.: New Numerical Results for the Optimization of Neumann Eigenvalues. In: Constanda, C. (ed.) Computational and Analytic Methods in Science and Engineering, pp. 1–20, Birkhäuser (2020)
2. Asante-Asamani, E.O., Kleefeld, A., Wade, B.A.: A second-order exponential time differencing scheme for non-linear reaction-diffusion systems with dimensional splitting. J. Comput. Phys. **415**, 109490 (2020)
3. Atar, R.: Invariant wedges for a two-point reflecting Brownian motion and the "hot spots" problem. Electron. J. Probab. **6**(18), 1–19 (2001)
4. Atar, R., Burdzy, K.: On Neumann eigenfunctions in lip domains. J. Am. Math. Soc. **17**(2), 243–265 (2004)
5. Atkinson, K.E.: The numerical solution of integral equations of the second kind, Cambridge University Press (1997)
6. Bañuelos, R., Burdzy, K.: On the "hot spots" conjecture of. J. Rauch. Journal of Functional Analysis **164**, 1–33 (1999)
7. Bass, R.F., Burdzy, K.: Fiber Brownian motion and the "hot spots" problem. Duke Mathematical Journal **105**(1), 25–58 (2000)
8. Beyn, W.J.: An integral method for solving nonlinear eigenvalue problems. Linear Algebra Appl. **436**, 3839–3863 (2012)
9. Burdzy, K.: The hot spots problem in planar domains with one hole. Duke Mathematical Journal **129**(3), 481–502 (2005)
10. Burdzy, K., Werner, W.: A counterexample to the "hot spots" conjecture. Ann. Math. **149**(1), 309–317 (1999)
11. Cakoni, F., Kress, R.: A boundary integral equation method for the transmission eigenvalue problem. Appl. Anal. **96**(1), 23–38 (2017)
12. Colton, D., Kress, R.: Inverse acoustic and electromagnetic scattering theory, 3rd edn Springer (2013)
13. Freitas, P.: Closed nodal lines and interior hot spots of the second eigenfunction of the Laplacian on surfaces. Indiana University Mathematics Journal **51**(2), 305–316 (2002)
14. Hempel, R., Seco, L.A., Simon, B.: The essential spectrum of Neumann Laplacians on some bounded singular domains. J. Funct. Anal. **102**(2), 448–483 (1991)
15. Jerison, D., Nadirashvili, N.: The "hot spots" conjecture for domains with two axes of symmetry. J. Am. Math. Soc. **13**(4), 741–772 (2000)
16. Judge, C., Mondal, S.: Euclidean triangles have no hot spots. Ann. Math. **191**(1), 167–211 (2020)

17. Kawohl, B.: Rearrangements and convexity of level sets in PDE. Lecture Notes in Mathematics, Springer (1985)
18. Kleefeld, A.: Numerical methods for acoustic and electromagnetic scattering: Transmission boundary-value problems, interior transmission eigenvalues, and the factorization method. Habilitation thesis, Brandenburg University of Technology Cottbus - Senftenberg Cottbus (2015)
19. Kleefeld, A.: Shape Optimization for Interior Neumann and Transmission Eigenvalues. In: Constanda, C., Harris, P. (eds.) Integral Methods in Science and Engineering, pp. 185–196. Springer (2019)
20. Kleefeld, A.: The hot spots conjecture can be false: Some numerical examples. arXiv:2101.01210, pp 1–31 (2021)
21. Kleefeld, A., Lin, T.C.: Boundary element collocation method for solving the exterior Neumann problem for Helmholtz's equation in three dimensions. Electron. Trans. Numer. Anal. **39**, 113–143 (2012)
22. Kleefeld, A., Lin, T.C.: A global Galerkin method for solving the exterior Neumann problem for the Helmholtz equation using Panich's integral equation approach. SIAM Journal on Scientific Compututing **35**(3), A1709–A1735 (2013)
23. Kleefeld, A., Pieronek, L.: The method of fundamental solutions for computing acoustic interior transmission eigenvalues. Inverse Problems **34**(3), 035007 (2018)
24. Krejčiřík, D., Tušek, M.: Location of hot spots in thin curved strips. Journal of Differential Equations **266**(6), 2953–2977 (2019)
25. Lagarias, J.C., Reeds, J.A., Wright, M.H., Wright, P.E.: Convergence properties of the Nelder–Mead simplex method in low dimensions. SIAM J. Optim. **9**(1), 112–147 (1998)
26. Lederman, R.R., Steinerberger, S.: Extreme values of the Fiedler vector on trees. arXiv:1912.08327 (2019)
27. McLean, W.: Strongly elliptic systems and boundary integral operators, Cambridge University Press (2000)
28. Miyamoto, Y.: The "hot spots" conjecture for a certain class of planar convex domains. Journal of Mathematical Physics **50**(10), 103530 (2009)
29. Miyamoto, Y.: A planar convex domain with many isolated "hot spots" on the boundary. Jpn. J. Ind. Appl. Math. **30**, 145–164 (2013)
30. Pascu, M.N.: Scaling coupling of reflecting Brownian motions and the hot spots problem. Trans. Am. Math. Soc. **354**(11), 4681–4702 (2002)
31. Rauch, J.: Lecture #1. Five Problems: An Introduction to the Qualitative Theory of Partial Differential Equations. In: Goldstein, J. (ed.) Partial Differential Equations and Related Topics, Lecture Notes in Mathematics, Vol. 446, pp. 355–369. Springer (1974)
32. Reed, M., Simon, B.: Methods of modern mathematical physics: vol.: 4.: analysis of operators, Academic Press (1978)
33. Sauter, S., Schwab, C.: Boundary Element Methods, Computational Mathematics, vol. 39 Springer (2011)
34. Seybert, A.F., Soenarko, B., Rizzo, F.J., Shippy, D.J.: An advance computational method for radiation and scattering of acoustic waves in three dimensions. Journal of the Acoustical Society of America **77**(2), 362–368 (1985)
35. Shampine, L.F.: Vectorized adaptive quadrature in MATLAB. J. Comput. Appl. Math. **211**(2), 131–140 (2008)
36. Siudeja, B.: Hot spots conjecture for a class of acute triangles. Math. Z. **208**, 783–806 (2015)
37. Śmigaj, W., Betcke, T., Arridge, S., Phillips, J., Schweiger, M.: Solving boundary integral problems with BEM++. ACM Transactions on Mathematical Software **41**(2), 6:1–6:40 (2015)
38. Steinbach, O., Unger, G.: Convergence analysis of a Galerkin boundary element method for the Dirichlet Laplacian eigenvalue problem. SIAM J. Numer. Anal. **50**(2), 710–728 (2012)
39. Steinerberger, S.: Hot spots in convex domains are in the tips (up to an inradius). Communications in Partial Differential Equations **45**(6), 641–654 (2020)
40. Tsai, C.C., Young, D.L., Chen, C.W., Fan, C.M.: The method of fundamental solutions for eigenproblems in domains with and without interior holes. Proceedings of the Royal Society A: Mathematical. Phys. Eng. Sci. **462**(2069), 1443–1466 (2006)
41. Yang, J., Zhang, B., Zhang, H.: The factorization method for reconstructing a penetrable obstacle with unknown buried objects. SIAM J. Appl. Math. **73**(2), 617–635 (2013)

Publisher's note Springer Nature remains neutral with regard to jurisdictional claims in published maps and institutional affiliations.